Effect of Cobalt and Nickel substitution on structural and dielectric properties of Magnesium ferrite nanoparticles

By

Mahpara Aslam

School of Chemical and Materials Engineering (SCME)

National University of Sciences and Technology (NUST)

2019

Effect of Cobalt and Nickel substitution on structural and dielectric properties of Magnesium ferrite nanoparticles

Name: Mahpara Aslam

Registration No: Fall 2016-MS NSE-04, 00000170559

This thesis is submitted as a partial fulfillment of the requirements for the degree of

Masters of Science in Nanoscience and Engineering

Supervisor Name: Dr. Iftikhar Hussain Gul

School of Chemical and Materials Engineering (SCME)

National University of Sciences and Technology (NUST)

H-12 Islamabad, Pakistan

April, 2019

Certificate

This is to certify that work in this thesis has been carried out by **Miss Mahpara Aslam** and completed under my supervision in Thermal Transport Laboratory, School of Chemical and Materials Engineering, National University of Sciences and Technology, H-12, Islamabad, Pakistan.

Supervisor: _____

Prof. Dr. Iftikhar Hussain Gul

Thermal Transport Laboratory
Materials Engineering Department
National University of Sciences and Technology, Islamabad

Submitted through:
Principal/Dean,
Materials Engineering Department
National University of Sciences and Technology, Islamabad

Dedication

I would like to dedicate this thesis to my beloved parents, my husband and my colleagues for their continuous help and support.

Acknowledgements

All praise and gratitude belong to *Allah Almighty* for giving me the strength and ability to understand, learn and complete this research work.

Special appreciation goes to my research supervisor Dr.Iftikhar Hussain Gul for his precious time and constant support throughout my work. This research could not have been possible without his invaluable guidance, constructive comments and suggestions throughout the experimental and thesis work.

I am also thankful to my family, friends and colleagues for their moral support, kindness and care. Thank you all very much.

Sincerely
Mahpara Aslam

Abstract

Nanoparticles of $Mg_{(1-2x)}$ (Co Ni)$_x$ Fe_2O_4, where x= 0.05, 0.10, 0.15, 0.20, 0.25 were synthesized by using sol-gel (auto-combustion) technique. X-Ray Powder Diffraction (XRD) for structural analysis, (FTIR) Fourier Transform Infrared Spectroscopy, Scanning Electron Microscopy (SEM) for morphological and surface analysis and Impedance Analyzer were used to investigate the dielectric properties of prepared samples. The XRD data patterns confirmed the formation of pure FCC (Face Centered Cubic) single phase spinel ferrite nanoparticles. The XRD data was used to calculate crystallite size for each sample and was in range from 59 ± 6nm. SEM results showed the uniformly synthesized nanoparticles. Octahedral and tetrahedral bands positions were confirmed using FTIR data. Dielectric properties were studied with the change of frequency at room temperature. Dielectric properties of prepared samples were found to be enhanced by increasing the cobalt and nickel content. The dielectric constant for pure magnesium ferrite was 43 which was increase 98% for the sample with highest cobalt and nickel content (x= 0.25) at 100HZ. Meanwhile increase of 99% was observed in dielectric loss and tangent loss values by increasing nickel and cobalt content. The increasing trend in AC conductivity was also observed with increasing frequency value. These results of AC impedance and electric modulus also suggested that this type of material can be investigated for supercapacitor, microwave absorbance applications.

Table of contents

List of Figures

Chapter 1: Introduction to Material

Chapter 2: Theoretical review

Chapter 3: Introduction to sample characterization techniques

Chapter 4: Results and Discussions

List of Tables

Chapter 1

Introduction to Material

Magnetic nanoparticles have great importance in scientific world due to their attractive properties in magnetic fluid, catalysis, data storage devices systems, magnetic resonance imaging, sensors, medical diagnosis etc. [1]. The area of research regarding magnetic nanoparticles has been the focus of scientists and researchers for over a decade. This is already known that the materials change their properties fascinatingly below specific size [2] and for the creative use of these magnetic nanoparticles study of their fundamental properties is essential. Magnetic particles mostly consist of iron, cobalt, nickel and their chemical compounds. There are different types of magnetic nanoparticles and Ferrites are the most explored magnetic nanoparticles. They exhibit their magnetic properties only when an external field is applied.

1.1 Introduction to magnetism

An atom is basic building unit of everything present in this universe. An atom is composed of electrons, protons and neutrons. Electrons moves in orbits around nucleus and also spin about their own axis. Being a moving charge, electrons produce small amount of currents and due to changing current generate very small amount of magnetic field, the magnetic moment of that existing magnetic field is always along its axis of rotation. The other magnetic moment produce is due to the spin motion of electron. It can only be in up or down direction. For completely filled shells the total magnetic moment is always zero. But for an unfilled shell it always has some value.

1.2 Classification of magnetic materials

Magnetic behavior of different materials can be classified in different types. The most commonly known types of magnetism are

- Diamagnetism
- Paramagnetism

- Anti-ferromagnetism
- Ferromagnetism

As shown in figure 1.1. Most of the elements of periodic table show diamagnetic behavior and metals in group I, group II and some of transition metals show paramagnetic behavior. The metals which show magnetic behavior in their elemental form are classified as ferromagnetic materials for example iron, cobalt and nickel.

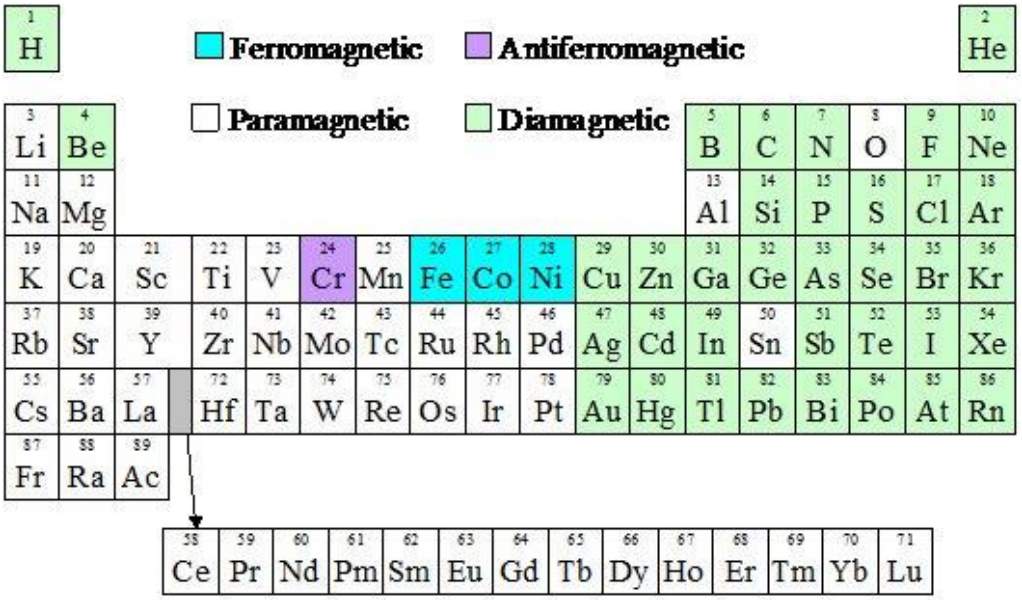

Figure 1.1: Room temperature magnetic behavior representation of each periodic table elements [3].

Ferrimagnetic behavior of elements cannot be seen in any pure elements but this behavior can only be found in complex compounds such as mixed metal oxides for example ferrites etc.

1.2.1 Diamagnetism

Diamagnetic materials have no net magnetic effect in the absence of applied field. But whenever an electric field (H) is applied the motion of spinning electrons starts aligning in the opposite direction of the applied electric field and the net magnetic moment of the

whole system becomes zero. All materials have diamagnetic effect to some extent, but in most of the materials it is very weak and got concealed by the higher value of paramagnetic behavior or ferromagnetic term. For all diamagnetic materials the susceptibility value is temperature dependent and does not vary which any change in temperature.

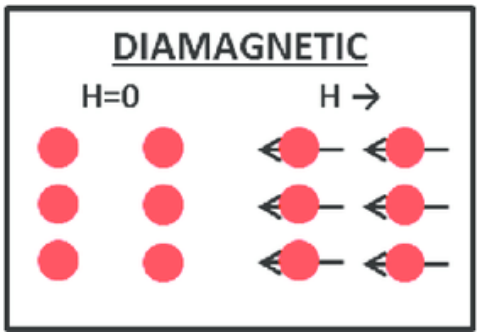

Figure 1.2: Atomic dipole ordering for diamagnetic materials. [4]

1.2.2 Paramagnetism

There are a lot of theories about Paramagnetism; those theories change from material to material and can only be valid for those specific materials. One of the theories is based on **Langevin Model**, according to this theory each atom has a separate magnetic moment and due to thermal agitation every magnetic moment is randomly oriented. But an externally applied field can creates can change the direction of the alignment of magnetic moments. When change of these alignments is in the direction of applied magnetic field it is called paramagnetic behavior. Temperature changes can greatly influence the alignment of magnetic moments. As the temperature increases it becomes harder for the magnetic moments to align in the direction of applied magnetic field due to the increase in thermal agitation. This also becomes reason of decrease in susceptibility. This behavior of paramagnetic materials can also be known as a **Curie Law**. This is represented as

$$\chi = \frac{C}{T}$$

Where C is known as material constant (curie constant). It is a material dependent quantity and varies from material to material.

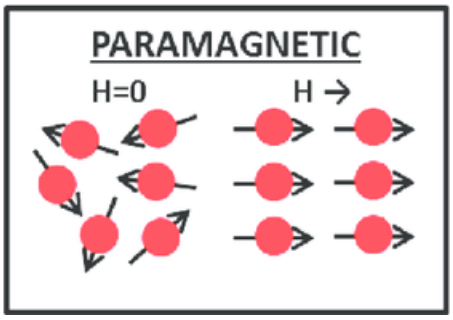

Figure 1.3: Atomic dipole ordering for paramagnetic materials. [4]

1.2.3 Ferromagnetism

In the view of classical theory the effect of Ferromagnetism can be describe as a presence of field inside a material that allows and helps the magnetic moments of atoms to interact and align parallel to each other.no outside filed is required for that alignment but that inbuilt filed is sufficient to magnetize the material to saturation. In their elemental form only iron, cobalt and nickel show ferromagnetic behavior at and above room temperature. With the increase in temperature the alignment of atomic magnetic moment mostly decreases and material becomes paramagnetic at high temperatures. This transitional temperature is called Curie temperature.

1.2.4 Anti-Ferromagnetism

The phenomena of anti-ferromagnetism is same as ferromagnetism. But the difference in this case is interaction of magnetic moments leads to the anti parallel alignment of them. All magnetic moments cancel the effect of each other and in result behave as a diamagnetic material. Chromium is the only material which shows this kind of behavior at room temperature. This behavior is also temperature dependent. By increasing the temperature increase in thermal movements changes the material to paramagnetic material above transition temperature. In this case this temperature is knows as **Neel** temperature.

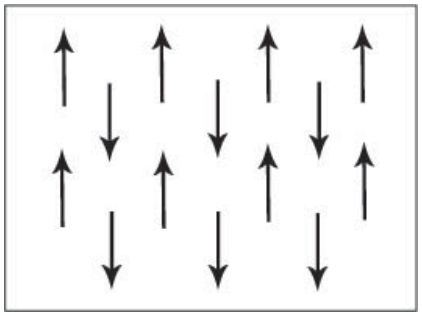

Fig 1.4: Ordering of dipoles for anti-ferromagnetism. [5]

1.2.5 Ferrimagnetism

The phenomena of ferrimagnetism can only be observed in more complex materials but not in elements such as oxides of metals etc. in the ferrimagnetic materials the both parallel and anti parallel alignments exists. In a part (domains) of crystal parallel alignment of magnetic moments occurs while in other parts (domains) anti parallel alignments occur. The overall effect results in a ferrimagnetism. This behavior is same as that of ferromagnetism but only occurs in compounds having complex crystal structure.

1.3 An overview of ferrites

Ferrite is a general term which is used for any magnetic oxide, in which iron oxide is a main component of their crystal structure. Fe_3O_4 also known as magnetite and also known to ancient people as a load stone was the first ever magnetic material to be recognized. Other magnetic materials which are discovered later ferrites are the most well-known ones. They are ferrimagnetic cubic spinel in nature and have combine properties of magnetic materials and electrical insulators. This is well known that the some properties of materials changes fascinatingly below a critical size and that's why study of Nano ferrites is essential for their creative use in devices.

1.3.1 Historical background of ferrites

The naturally occurring ferrites Fe_3O_4 aroused the scientific curiosity of man. The ancient people living in 600 B.C. believed that load stone (magnetite) possesses an inherent living force which accounts for the observed attraction between magnetite and iron. The first ever measurement of the magnetization of magnetite was done by Du-Bois (1890).

However Hilpert (1909) was the first to prepare ferrites having general formula ($MOFe_2O_3$) [6]. This this formula M= divalent metal ion an O representing the oxygen atoms.

First ever X-ray analysis of magnetic particles was done by Barth and Posnjak through which they discovered inverted spinel structure, essential for the existence of the ferromagnetic properties of ferrites. In 1930 Holland became the center of extensive work in the field of ferrites and the importance of accurate oxygen content for the quality of ferrite to be used at high frequency was shown for the first time [7]. Verwey reported that electronic conductivity of ferrites which is mainly represents the hopping of electrons between Fe^{+2} /Fe^{+3} ions. The ferrite with inverted spinel structure was shown to be ferrimagnetic where as normal spinel structure ferrite to be nonmagnetic.

In 1948 Neel published the explanatory theory on the origin of magnetism in ferrites in then modified his theory in 1952 [8]. The experimental proof of Neel's theory was established by Gorter and Gaillard by measuring the magnetization of the mixed ferrites. Shull and Strauser confirmed the Neel's theory for magnetite and Zinc ferrite with the help of neutron diffraction studies. Koop's studied high conductivity in ferrites and then associated this with high dielectric constant and obtained the formula [9]. First international conference of ferrites was conducted in 1980 in which Prof Takieo suggested the use of ferrite material as a power ferrite. In the respective years a lot of work is happening regarding synthesis and usage of ferrite materials in devices.

1.3.2 Soft ferrites

Soft ferrites are those which can be easily magnetized and demagnetized by the application and removal of applied field. They can only remain magnetized when they are in the influence of magnetic field. For soft ferrites the value of hysteresis loop and coercivity is very low. Which means that the material magnetization can easily reverse direction without losing much energy [10]. An ideal ferrite would have

- Low value coercivity
- Large value of saturation magnetization
- Zero value remanence
- zero hysteresis loss value

- Large permeability [11].

1.3.3 Hard ferrites

They are also known as **Ceramic Magnets**. In case of hard ferrites magnetization of material remain retained even after the removal of applied field. They have large hysteresis loop as well as high value of coercivity. Oxides of iron, barium and strontium shows behavior of hard ferrites.

1.4 Composition of ferrites

Ferrites has general chemical formula M^{+2} Fe_2^{+3} O_4^{-2} where M= divalent metal ion for example

- Nickel ion (Ni^{2+})
- Zinc ion (Zn^{2+})
- Magnesium ion (Mg^{2+})
- Cobalt ion (Co^{2+})
- Copper ion (Cu^{2+})
- Iron ion (Fe^{2+})

Whenever we talk about the mixed ferries it means that we can have a combination of different ions. Other combinations of equivalent valency are possible.

1.5 Structure of ferrites

In 1915 W. H. Bragg determined the structure of spinel ferrite for the very first time along with Nishikawa [12]. The crystal structure of ferrites was same as that of mineral spinel (MgAl2O4) and that's why named after that. The structure of spinel ferrite is the simplest one.it consists of 32 closely packed oxygen ions in a unit cell. They have packed between two kinds of interstices in FCC lattice of anions. In figure 1.4(a) where, solid lines and the dotted lines represent the top and bottom layers of oxygen spheres respectively.

To form a spinel structure the ionic radius of divalent metal ion M must be less than or about 1 Å. And most of the divalent metal ions (listed above) that form spinel structure have their ionic radius between 0.6 to 1Å [13]. If the ionic radius of M is greater than 1 Å then the electrostatic Coulomb force required for the stability of crystal are insufficient. For examples Ca^{+2} (ionic radius 1.06 Å) does not form spinel crystal, where in Mn^{+2}

(0.91 Å) does form spinel crystal. In figure 1.4, it can be seen that there are two kinds of interstices are present, denoted by letter (A) (tetrahedral site) and (B) (octahedral site).

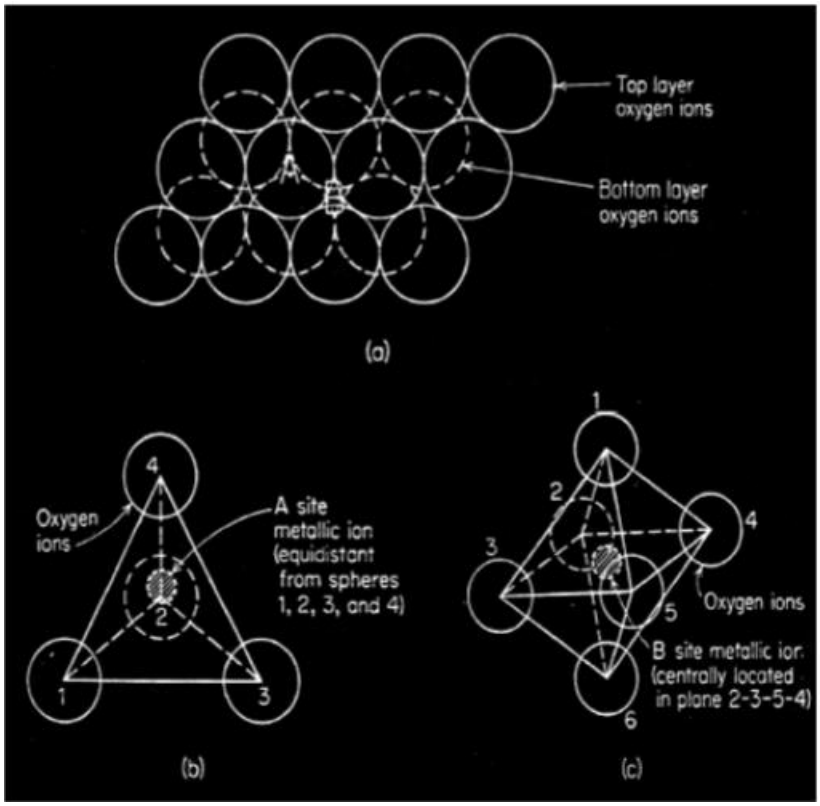

Figure 1.5: Ionic positions (a) Hexagonal Close packing (b) Tetrahedral (A) site (c) Octahedral (B) site [14].

There are total 96 interstices are formed in spinel structure, 24 of them are filled by a cations, the remaining 72 remains empty. The site occupied by the cations are of two kinds known as tetrahedral or (A) sites and octahedral or (B) sites. The (A) site only contain eight interstices are which are occupied and on A site each one is surrounded by 4 Oxygen atom and on the (B)site, sixteen are occupied and each one is surrounded by six oxygen ions [14] as shown in figure 1.4(b) and figure 1.4(c).

1.6 Classification of ferrites

The ferrite can be classified by their crystal structure type. They consist of three different structures, Hexagonal, Garnet and Spinel. Hexagonal ferrites are important in permanent magnetic applications, magnetic garnets. Garnets have special applications in microwave devices and spinel ferrites are important in many electrical, electronic, automobile, computer applications.

1.6.1 Garnet

Garnets have chemical formula of $M_3Fe_5O_{12}$ crystal where M can be (yttrium (Y), rare-earth) ion for example.

- Gadolinium (Gd)
- Terbium (Tb)
- Dysprosium (Dy)
- Holmium (Ho)
- Erbium (Er)
- Thulium (Tm)
- Lutetium (Lu)
- Europium (Eu)

Their chemical formula can also be written as $(3M_3O_3)$ c $(2Fe_3O_3)$ a $(3Fe_2O_3)$ d the superscripts c, a, d, refer to dodecahedron (12 -coordinated), octahedron and tetrahedron respectively. The structure of garnets is same as that of silicate mineral (garnet). The net ferrimagnetism in garnets is very complex because of the presence of anti-parallel spin alignments among all the three sites. They are hard ferrites magnetically.

1.6.2 Hexagonal ferrite

The general formula of hexagonal ferrites is $MFe_{12}O_{19}$, where M represents divalent ion usually Ba, Sr, or Pb (barium strontium or lead). Their structure is related to the spinel structure in which the oxygen lattice, being Fcc consists of series of hexagonal layers of oxygen lying perpendicular to the (111) direction. Their crystal structure is very complex. That can be described as hexagonal lattice with additional (vertical) c-axis. Hexagonal ferrites mostly magnetize along this axis easily and their direction of magnetization cannot be easily changeable to another axis. Hexagonal lattice consist of three different lattice sites which are occupied by metal ions.

- Tetrahedral site

- Octahedral site
- Trigonal-bi-pyramid

Each side of metal ions is surrounded by 6 oxygen ions. Their crystal as well as magnetic structure of hexagonal ferrites are remarkably complex and cannot be easily described.

1.6.3 Spinel ferrite

Spinel ferrites are soft ferrites means they can easily change their direction of magnetization by applying external field. They have cubic in structure. In spinel ferrites the distribution of metal ions (divalent/trivalent) at both octahedral and tetrahedral sites can greatly influence their properties. Barth and Ponjak observed the different arrangement of cations in spinel ferrites. And on the basis of different cationic distribution they can be categorized differently as [15].

- Normal spinel
- Inverse spinel and
- Random spinel ferrite

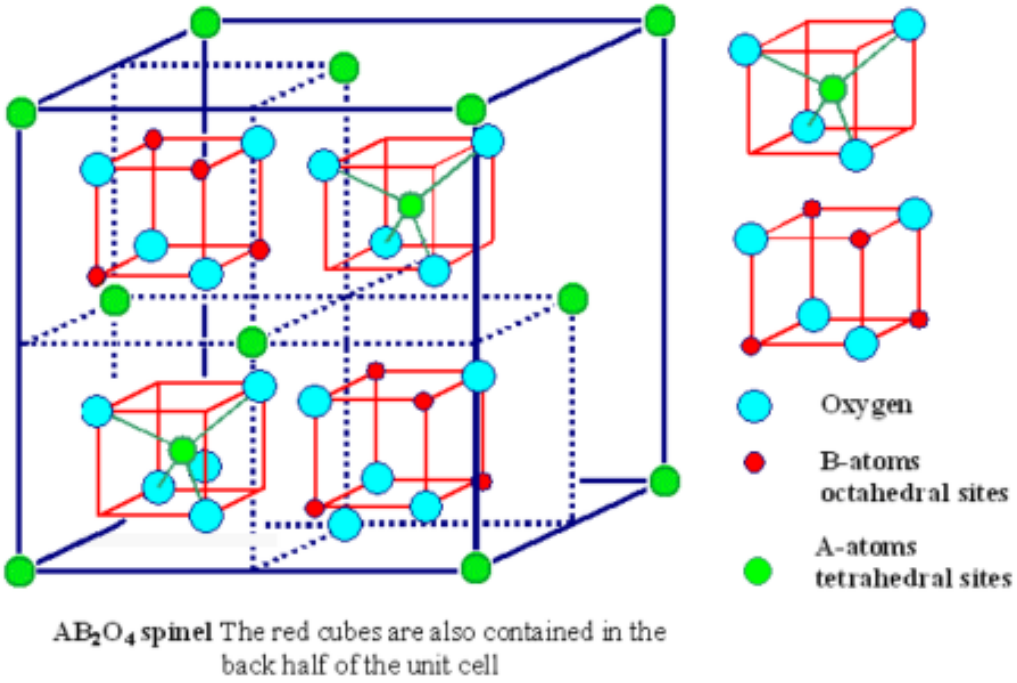

AB_2O_4 **spinel** The red cubes are also contained in the back half of the unit cell

Fig 1.6: Unit cell of spinal ferrites showing tetrahedral and octahedral sites [16]

1.6.3.1 Normal spinel ferrites

In normal spinel ferrites, divalent metal ions occupy (A) sites and trivalent metal ions occupy (B) sites. These type of spinel ferrite have no A-B interactions because (A) site do not contain any magnetic ion. They only contain B-B interactions, in which half of the magnetic ions lines up in one direction and other half in other direction which leads nonmagnetic ferrites. ZnFe2O4 and CdFe2O4 are the examples of normal spinel ferrites.

The cationic distribution for normal spinel ferrite is given by

$$(M^{+2})A\ (Fe^{+3})\ B\ O_4^{2-}$$

Where, M=divalent metal ion.

1.6.3.2 Inverse spinel ferrites

In case of inverse spinel ferrites, one trivalent ion (Fe^{+3}) resides at the tetrahedral (A) site while the other remaining trivalent ions resides at (Fe^{+3}) and the all divalent metallic ions M^{+2} resides at the (B) site. They are the simplest ferrites and the common examples of inverse spinel ferrites are MnFe2O4, CoFe2O4 and NiFe2O4.

The cationic distribution for inverse spinel ferrite is given by

$$(Fe^{+3})A\ (M^{+2}\ Fe^{+3})B\ O_4^{-2}$$

1.6.3.3 Random spinel ferrite

In the case of random spinel ferrites M^{+2} and Fe^{+3} are randomly distributed at tetrahedral and octahedral sites that the reason they are classified as random spinel ferrites. Examples contain copper ferrites etc. The distribution of random spinel ferrites depends upon the process of synthesis and sintering process.

The cationic distribution of random spinel ferrite is given by

$$(M_\delta^{2+}\ Fe_{1-\delta}^{3+})A\ (M_{1-\delta}^{2+}\ Fe_{1+\delta}^{3+})B\ O_4^{2-}$$

1.7 The cation distribution

The cationic distribution in spinel ferrites has great influence on electrical and magnetic properties. The distribution of Fe and the M^{+2} among the octahedral and tetrahedral sites of the spinel lattice depends on many factors. The cationic distribution can be determined by several methods. Some of them are

- X-ray diffraction methods [17]
- Neutron diffraction method
- Mossbauer spectroscopy [18]
- Magnetic susceptibility measurement
- Infrared absorption spectroscopy [19]

In X-ray diffraction method, X-ray intensity ratio calculations are made for the planes (220), (311), (400), (440) etc. Then these theoretical and experimental values of X-ray intensity ratio are compared. The combination for which cations theoretical and experimental values seems close to each other is taken as correct cationic distribution.

1.8 Factors effecting cationic distribution

Some of the factors are listed below which can influence the cationic distribution at tetrahedral and octahedral sites.

- ionic radius
- electronic configuration
- method of preparation

1.8.1 Ionic radius

In spinel lattice, the octahedral (B) site has large ionic radius then tetrahedral (A) site, therefore the large cations like Co^{+2} and Ni^{+2} generally will prefer to occupy the octahedral (B) sites while the small cations will occupy the (A) tetrahedral sites.

1.8.2 The electronic configuration

It is a common observation that ions with filled d-shell often have tendency to form sp^3 hybrid orbital and occupy the tetrahedral (A) sites for example Zn^{+2} and Ge^{+4}, whereas the ions with d^3 and s^8 electronic configuration have a tendency to form d^3 sp^3 hybrid orbital and occupy the octahedral sites in spinel. For example Cr^{+3} and Ni^{+2} [20].

1.8.3 Method of preparation

It is observed that method of preparation can also effect the cationic distribution of at tetrahedral sites and octahedral sites. The cationic distribution strongly depends on heat treatment (sintering) of the material. Materials with same composition prepared by two different methods can have different properties.

1.9 Applications of ferrites

The spinel ferrites have great potential for applications in different fields. Even after a lot of research work been done in the field of ferrites the scientist and technologist are still interested in ferrite materials. The recent interest of the researchers is focused on the ferrites doping. Which can be prepared using various compositions, synthesis routes and with different cationic concentrations which highly affects the properties like electrical, dielectric and magnetic of the material. Ferrite materials are important magnetic materials and have applications in power conditioning, electromagnetic device, electromagnetic wave absorbers, magnetic inks for bank cards, and recording media etc. Some of the major fields of applications of ferrites are listed below

- Medical diagnostics and treatments
- Drug delivery
- Magnetic shielding
- Magnetic sensors
- Electromagnetic interference suppression
- Pollution control
- High frequency applications

1.10 Objectives of this research

The objectives of this research work are as follows

- Preparation of $MgFe_2O_4$ single phase spinel nanoparticles using sol gel synthesis.
- Preparation of CO and Ni substituted $Mg_{(1-2x)}(Co\ Ni)_x Fe_2O_4$, x= 0.05, 0.10, 0.15, 0.20, 0.25 nanoparticles.
- Material characterization using XRD, FTIR and SEM.
- Study the effect of dopant concentration in structural and dielectric properties.

Chapter 2

Theoretical review

Synthesis of nanoparticles can be done by using two major approaches.

1- Top down approach
2- Bottom up approach

The top down approach is a processes in which we starts from large structures and subsequently using finer methods forms more smaller and finer structures which includes lithography, ball milling, laser ablation, electro spinning, arc discharge etc. while the bottom approach is one in which atoms, molecules and clusters are combined together to form nanoparticles. Examples of bottom up approach are wet chemical synthesis, chemical vapor deposition (CVD), hydrothermal synthesis, physical vapor deposition (PVD), MBE, self-assembly etc.

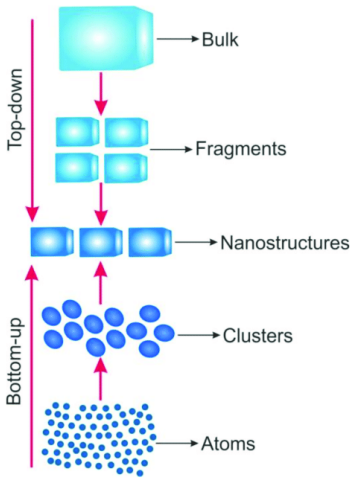

Figure 2.1: Top down and bottom up approach

Both techniques have some advantages and disadvantages. In top down approach it is difficult to attain homogenous nanoparticles and of smaller size and also a significant amount of impurity is always present. While in the use of bottom up technique implementation cost is likely to be higher. There are different methods for the synthesis

of nanoparticles. Each method has its own advantage and disadvantages. Some of the methods are shown in the following figure.

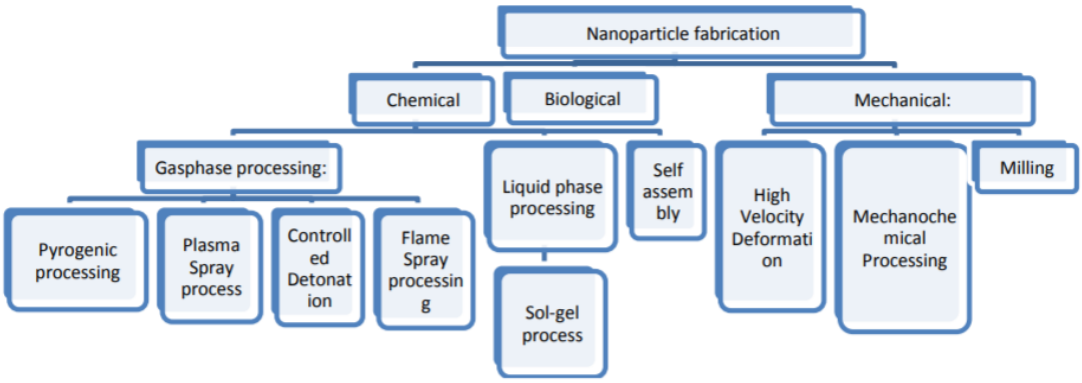

Figure 2.2: Scheme of fabrication of Nanomaterials techniques.

Ferrites nanoparticles synthesis can be carried out using different routes for example hydrothermal[21], solvothermal[22], co precipitation[23], sol gel, micro emulsion and other methods. Properties of synthesized ferrite greatly depends on synthesis route and change with synthesis conditions. A lot of work in the regard of synthesis of ferrites has already been done and still carried out for different applications.

2.1 Chemistry of Sol-gel synthesis

2.1.1 Introduction

The sol gel synthesis is kind of inorganic polymerization. It was firstly described by Ebelmann in 1864 [24]. As in practice, sol-gel synthesis looks a very simple process that it requires just one step to get a required product but at microscopic as well as nanoscopic scale it is such a complex technique that it goes through several transformations of different nature before we get desired results.

A sol consist of colloidal suspension, in which solid particles (solute) are dispersed in some liquid medium (solvent).The common precursors mostly used for sol–gel synthesis are

- **Inorganic salts (chlorides, nitrates)**
- **organic compounds**

The sol–gel process involves hydrolysis and condensation of metal precursors which leads to the formation of a three dimensional inorganic network. In ferrites, Colloidal

solution is composed of chemicals like metals or metalloids0surrounded by0ligands for example nitrates of metals. The nitrates salts are easily soluble by in water. This process is called hydrolysis. In this process hydroxyl ion attached to the metal ion (M) as shown in the below reaction.

$$\boldsymbol{M(OR)_4 + H_2O \rightarrow HO - M(OR)_3 + ROH}$$

On the completion of hydrolysis all OR groups replaced by OH

$$\boldsymbol{M(OR)_4 + 4H_2O \rightarrow M(OH)_4 + 4ROH}$$

Here could be another scenario, when hydrolysis stop while the metal is partially hydrolyzed M $(OR)_{4-X}$ $(OH)_X$. These two molecules can take part in condensation by linking together. This process liberate water molecule as shown in below reaction.

$$\boldsymbol{(OR)_3M - OH + HO - M(OR)_3 \rightarrow (OR)_3M - O - M(OR)_3 + H_20}$$

This type of continuous reaction builds large metal containing molecule which is called gel. It contains a continuous solid structure which is amorphous in nature but can be crystallized on heating treatment. For the preparation of ferrites sintering of the prepared samples need to be done at elevated temperatures.

A flow chart of sol-gel auto combustion method is shown in figure 3.3.

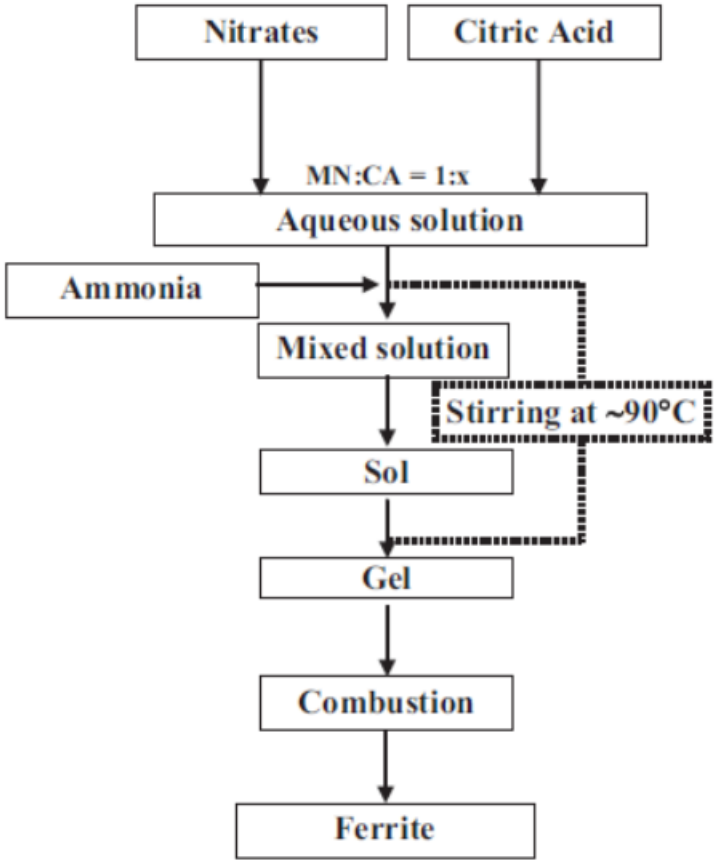

Figure 2.3: Flow chart of sol-gel combustion method.

2.1.2 Effect of different factors on Sol-gel synthesis

Many factors can affect the structure, morphology, particle size etc. during the synthesis. Some of them are listed below

- Effect of chelating agent
- Effect of pH

2.1.2.1 Effect of chelating agent:

For the synthesis of powder ferrite nanoparticles precursors (metal nitrates) and chelating agent (urea/ citric acid [25] /glycine/hexamethylenetetramine etc.) is used. Mostly the ration of metal nitrates and citric acid is kept at 1:3. The ratio and type of chelating agent greatly influence the structural and magnetic properties, cationic distribution and particle size [26]. The combustion process in each chelating agent occurs differently. In case of

hexamethylenetetramine and glycine the process of auto combustion took only few seconds. In case of citric acid and tartaric acid the whole combustion processes took more than 30 minutes. While in case of urea it took 2-3 minutes to complete auto combustion process [27].

2.1.2.2 Effect of pH

In sol-gel synthesis the pH value of the solution is controlled by ammonia. It catalyze the process for hydrolysis and then condensation.ph values greatly influence the combustion rate [28]. pH values between (7-8) induce a fast gelation, which is ideal for making small size nanoparticles. While pH values between (2-3) induce low gelation and ideal for making extended network.

2.2 Literature study

Ferrites are good dielectric materials that's why they have long range of applications for example in microwave devices, targeted drug delivery [29], data storage sensors [30], catalysis [31], core materials and electromagnetic absorbers [32] etc.

Gul et al. prepared Co_{1-x} $Ni_xFe_2O_4$ nanoparticles, by co precipitation, while x varying from 0.0 to 0.5. The particle size determined was in between 14nm to 21nm. It was observed that the increase in the nickel concentration decreased the value of saturation magnetization and coercivity. As the magnetic moment of nickel ions are low (2μB) than that of cobalt ions (3μB) so this trend of decreasing magnetization was attributed to the increase in nickel ions at octahedral sites [33].

Pardeep et al. synthesized $MgFe_2O_4$ nanoparticles using sol-gel (wet chemical) route. They have done XRD, SEM and FTIR analysis which confirms single phase and crystalline prepared samples. They also studied the distribution of cations theoretically and concluded that this distribution can cause change in structure and other properties. They also reported the decrease in the value of magnetic moment and saturation magnetization with respect to the bulk ferrite [34].

Smitha et al. prepared magnesium ferrite nanoparticles using the sol gel method. The XRD data and FTIR results confirms single phase of spinel structure formation with no impurity present. The temperature variation of dc conductivity was also studied and reported the Decrease in conductivity occur till temperature 323K because of the water absorbed in the sample. According to the magnetic studies reveals that the sample shows ferromagnetic behavior at low temperature [35].

Bortnic et al. synthesized $CoFe_2O_4$ nanoparticles by cheap and nontoxic sol-gel route. Pectin used as gelation agent and sucrose as poly- condensation agent. XRD analysis and FTIR data was collected which confirmed the single phase spinel structure formation. Grain size was 20-75nm which was calculated using TEM [36].

Thankachan et al. synthesized Magnesium ferrite nanoparticles by using both co-precipitation and sol-gel route. XRD analysis showed average crystallite size of 9nm by sol-gel synthesis and comparatively larger 12nm crystallite size for co precipitation method. And both synthesis techniques confirmed the single phase spinel structure through XRD and FTIR. The magnetic measurement shows both samples to be ferrimagnetic with a hysteresis. The saturation0magnetization value for the co-precipitation sample is very low when compared with the sol-gel sample. The low value of remanent ratio shows isotropy of the co-precipitation route prepared sample. The measurement of dielectric constant and dielectric loss value with variation of frequency was in accordance with Maxwell–Wagner theory. It is reported that the dielectric and ac conductivity values are temperature dependent [37].

Moradmard et al. synthesized $Ni_{1-x}Mg_xFe_2O_4$ by using co precipitation route. The X-ray diffraction analysis confirmed the formation of single phase structure and it is observed that by adding magnesium overall crystallite size increases. Magnetic properties and dielectric properties were also studied Magnetic measurement shows increase in magnesium reduce magnetization and increase coercivity value. Increase in coercivity is related to the replacement of Fe^{+3} by Mg^{+2} ions at octahedral sites. The dielectric properties like dielectric constant were investigated. Decrease in the dielectric

values has been reported. Koop's theory explains the decrease in dielectric loss value with increase in frequency [38].

Mahalakshmi et al. prepared nickel ferrite nanoparticles ($Ni_x\ Fe_{3-x}\ O_4$). They reported the decrease in dielectric values and increase in dielectric loss values. The report also shows the dependence of ac conductivity on nickel concentration as it is was only dependent on the conduction of electrons between Fe^{+2}/Fe^{+3} ions but also on Ni^{+2}/Ni^{+3} ions. Conductivity values increased with the increase in frequency [39].

Hashim et al. studied the effect of cr+3 doping in Ni-Mg ferrite nano particles. Prepared materials were analyzed using XRD, FTIR and Scanning electron microscopy. They have confirmed the mixed spinel nature of the material. They have reported that increase in Cr^{+3} content cause decrease in lattice constant values. which was expected because the radii of Cr^{+3} is less than Fe^{+3}. The magnetic analysis shows a decrease in saturation magnetization. Which explains the low exchange at A and B site [40].

Velhal et al. synthesized $Co_{1-x}\ Ni_x\ Fe_2O_4$ successfully by using simple sol-gel route. The crystalline structure was confirmed using xrd analysis while little impurity was also observed of phase Fe2O3. They have reported that the increase in nickel content not only improves crystallite size but also improves the value of magnetization. The general trend of dielectric constant and dielectric loss was seen which was decreasing with frequency. Increase in magnetization and decrease in coercivity was observed and their behaviuor was temperature dependent.[41].

Rani et.al studied the dielectric and structural properties of zinc doped cobalt ferrite nanoparticles. The samples were prepared by using simple solution combustion method. [42]. Structural analysis of samples was done by using XRD, which confirms the cubic spinel nature and nm crystallite size of prepared samples. Particle size was calculated using TEM analysis. In dielectric studies a decrease in dielectric constant values was reported after 0.2 Zn values which is due to the increase of Zn^{+2} at octahedral B sites. Same trend was also been observed for tangent loss values.

R. B. Bhise et al. studied electric, structural, magnetic and dielectric properties by using cobalt doped zinc ferrite by simple sol gel method. Those samples were sintered at two different temperatures and characterized by XRD, FTIR and SEM. The XRD analysis confirm the phase structure and calculated particle size using SEM. Increase in saturation magnetization was reported by the increase in cobalt content as well as by increasing the sintering temperature. Decrease in impedance was reported due to lowering of magnetostriction constant [43].

K. Vijaya Kumar et.al synthesized copper sunsituted nickel ferrites nanoparticles with series of different compositions of copper. Citric acid was used as a fuel for combustion in sol gel synthesis. Crystallite size was measured using XRD data which was in range of 40-60nm. This analysis also confirms the cubic spinel nature of material. electrical resistivity of the prepared sample was repotedly increased by increasing the copper content. [44].

H.S. Singh et al. worked on ferrite nanoparticles due to their remarkable dielectric and electric properties. They worked on nickel ferrite and substituted nickel ferrite. The magnetic, electric and physical properties of nickel showed a remarkable improve when it is substituted with Aluminum. So it can be concluded that the properties can be enhanced by making composite of nickel with other material. The study is needed to know the exact amount of substitution and method of preparation. The effect of preparation technique should also be known.[45]

Y.C yang et al. studied nickel ferrite and its electrical, magnetic and structural properties. Also composite of nickel ferrite with transition metals and rare earth metal was studies. The particles were prepared by different routes including sol-gel method and co precipitation method and a comparison id made between them. The particles prepared by sol-gel method were big in size, highly resistive, ferromagnetic and multi domain. The prepared particles can be used in applications involving high frequency. The particles prepared by co precipitation method were smaller in size, paramagnetic and had single domain. The prepared particles are applicable in magnetic resonance imaging, drug delivery, medical applications etc. when nickel ferrite is doped with rare earth element

the reduction in magnetization is observed. The increase in coercively is observed by adding transition metal. The decrease in dielectric loss is observed when doped with rare earth metal ions. Particle size increase in case of doping with transition elements. The lattice constant is also observed to increase with doping. The unit cell is also observed to expand. Further studies suggested that dielectric and electrical properties, for example dielectric loss of doped nickel ferrite is observed to decrease and resistivity is observed to increase by doping with transition metals [46].

2.3 Synthesis of $Mg_{1-X}(Co\ Ni)_X Fe_2 0_4$

For the preparation of composition $Mg_{1-X}(Co\ Ni)_X Fe_2 0_4$,where x=(0.0, 0.05, 0.10, 0.15, 0.20, 0.25) sol gel synthesis technique has been used.

2.3.1 Apparatus used

- Beaker
- Magnetic stirrer
- Heating plate
- Permanent magnet
- Spatula
- Mortar and pestle
- China dishes

2.3.2 Materials used

- Iron nitrate [$Fe(NO_3)_2.9H_2O$]
- Magnesium nitrate [$Mg(NO3)_{2]}$
- Cobalt nitrate [$Co(NO_3)_2.6H_2O$]
- Nickel nitrate [$Ni(NO_3)_2.6H_2O$]
- Citric acid [$C_6H_8O_7$]
- Ammonia [NH_4OH]
- Deionized water

All the above mentioned materials were analytical grade and was provided by ACROS organics, Sigma Aldrich and EMSURE®.

2.3.3 Procedure

For sol gel synthesis metal nitrates and citric acid ratio was kept as 1:3 and following stoichiometric ratio formula was used to calculate the composition of different chemicals utilized in the process.

$$\boldsymbol{mass\ (g) = \frac{molarity X\ molecular\ mass\ X\ 100}{1000}}$$

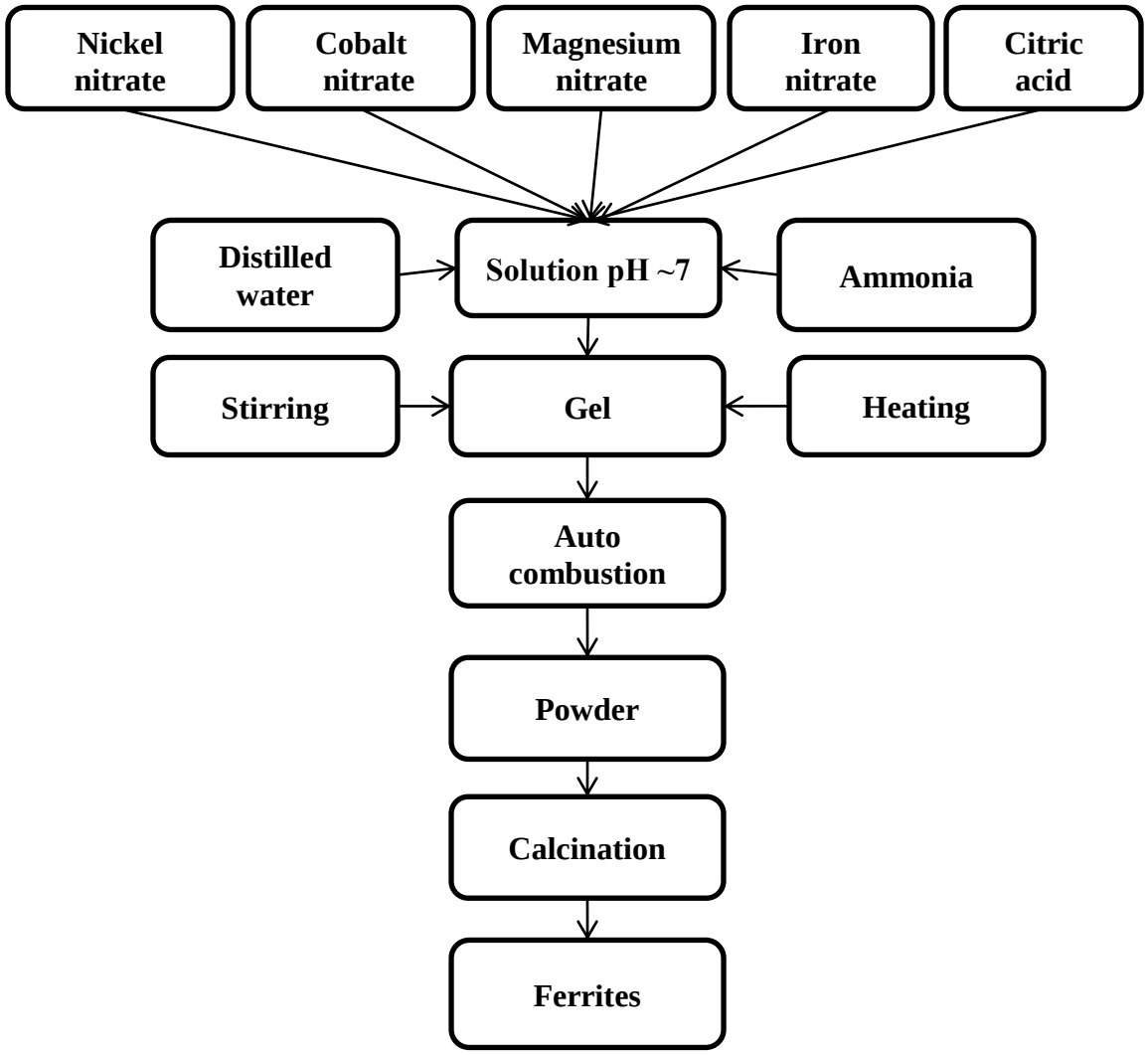

Figure 2.4: Flow chart diagram for the synthesis of ferrites samples preparation.

Each starting material magnesium nitrate, iron nitrate and citric acid (3M) were dissolved in stoichiometric amount in 100ml of deionized water. Each solution was magnetically stirred for at least 15 minutes until they form a clear solution. Then after combining all the solutions together ammonia was added drop wise until the mixture pH changed to (7-7.5) and also changed its color to dark green. Then the mixed solution was kept onto hot plate with continuous stirring at 100°C. Due to continuous evaporation the solution become viscous and formed a dark brown color viscous gel. After the removal of all water molecules the gel ignited and burnt and burning continued until the whole citric acid is consumed. After the completion of combustion greenish brown color ashes are formed. Ashes are then collected using spatula and grinded using mortar and pastel and then sintered at 800°C in muffle furnace.

For the synthesis of nickel and cobalt doped samples, nickel nitrate and cobalt nitrate was also added in the mixture in a measured stoichiometric ration along with magnesium nitrate, iron nitrate and citric acid. After that the same procedure was followed to form ferrites samples.

Chapter 3

Introduction to sample characterization techniques

The properties of synthesized $Mg_{(1-2x)}$ (Co Ni)$_x$ Fe_2O_4 are analyzed by performing some specific analysis techniques. Properties like physical and chemical properties and other information about material such as morphology, lattice parameter, structure etc. can be obtained using one of the analysis techniques. This chapter will cover a short introduction of the characterization techniques. Following characterization techniques can be used for the analysis of synthesized composite.

3.1 X-Ray diffraction technique

It is a useful tool for the identification of degree of crystallinaity and structure of a material. Clear information about structural strain, crystal defects, average crystallite size, crystallographic orientation and degree of crystallinaity can be obtained by using XRD. Three different methods can be used for finding out crystal structure i.e. powder diffraction method, Laue method and rotating crystal method. Two techniques can be used to determine crystal size if powder diffraction method is used. Those techniques are as follows.

- Debye Sherrer Method
- Diffractometer method

The sample was in the form of fine grinded powder. Copper, Molybdenum etc. can be used as a target material. Cu (k-Alpha) 1.54060Å source was the XRD source used for analysis in this case.

3.1.1 Basic principle of XRD

The powdered sample is placed for analysis. X-ray beam is made to fall on the sample and reflected from plane of crystal. The crystal plane reflects the X-rays that are incident

on material. The interference only takes place when incidence angle is exactly same as reflection angle. The Bragg's Law is given by

$$n\lambda = 2dSin\theta$$

where n=1,2,3….. Representing order of interference, θ is incidence angle, d is Interlayer distance and λ is incident X-ray wavelength. The Bragg's law states that the incident ray is reflected only when the path difference between set of planes is integral multiple of 2dsinθ [47]**.** The set of planes are at an equal distance of d.

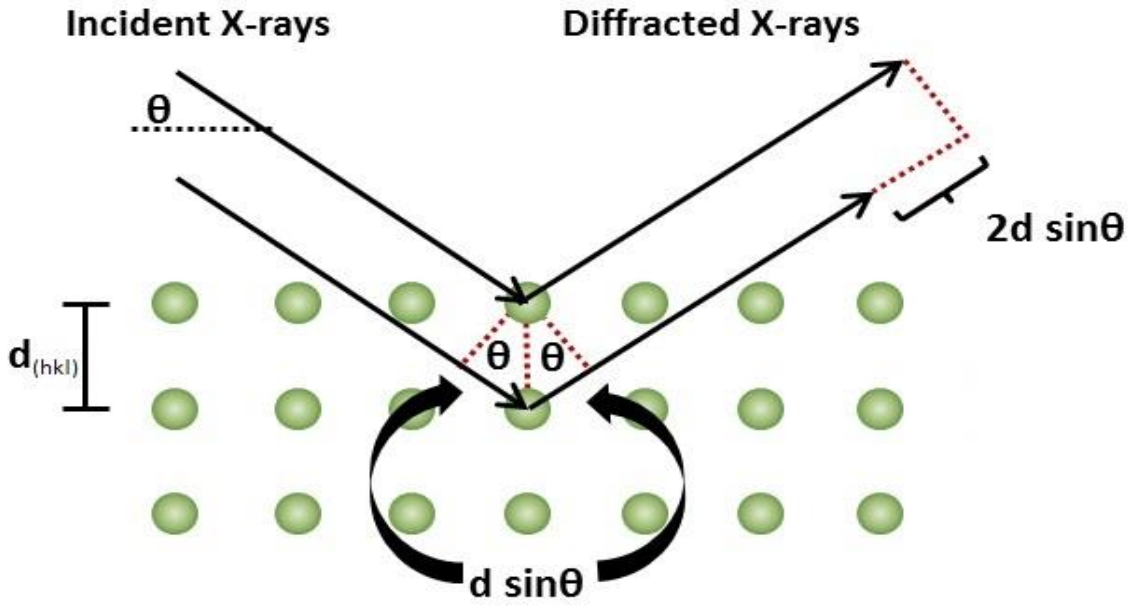

Fig 3.1 Incident x-ray beam scattered by atomic plane in a crystal [48]

The equation is known as Bragg's equation. The condition for reflection in above mentioned equation is that it only occur when θ<2d. For this reason visible light cannot be used. For the characterization of a three dimensional structure three techniques are usually used which are as follows:

- Laue Method
- Powder method
- Rotating Crystal Method

The sample which is to be characterized using XRD is in the form of Nano powder. So the powder method will be the one useful for the desired sample. For the evaluation of powdered sample and in the case of in availability of single crystal of acceptable size, powder diffraction is the best method to be employed. The procedure of this experiment includes the crushing of sample in to fine powder. Afterwards the sample will be placed in aluminum or glass rectangular shaped plate. A monochromatic X-ray beam is then directed towards the powdered sample.

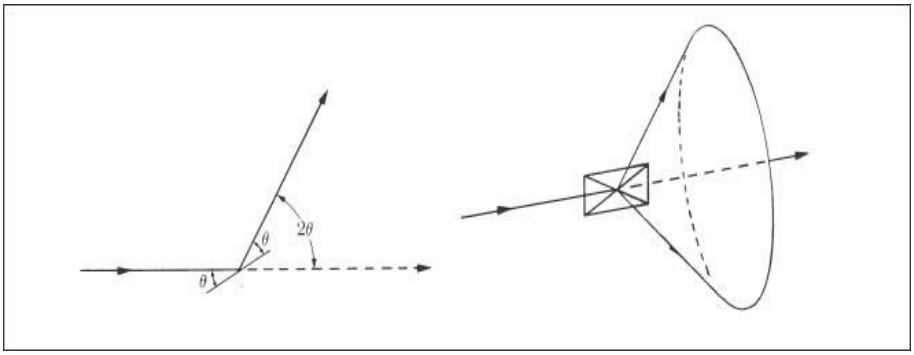

Fig 3.2 Diffracted cones of radiations forming in powder method [48]

Consider the reflection as shown in figure. The fraction of sample, which is in powder form, is at such an orientation which will enable reflection by being present at correct Bragg angles. When the plane is rotated about the beam which is made incident, the path of motion of reflected beam will be across the surface of cone. In the case of our particles the reflection does not occur across the surface, a large number of crystal particles will have same reflections and some of those reflections will be able to satisfy brags law. The inter planner spacing, d, can be calculated by knowing values of λ and θ.

3.1.2 Lattice constant

Lattice constant defines the unit cell of a crystal. It is the length of one edge of the cell or an angle forming between edges. It can also be termed as lattice constant or lattice parameter. The distance, which is constant, between the lattice points is known as lattice constant. Following equation is used to calculate lattice constant.

$$\boldsymbol{a = \frac{\lambda\,(h^2 + k^2 + l^2)^{1/2}}{2Sin\theta}}$$

In the above equation, lattice constant is “a”, the wavelength of X-ray radiation is 1.54060Å for Cukα, miller indices are “h, k, l” and diffraction angle is θ.

3.1.3 Crystallite size

For the identification and confirmation of the experimentally obtained diffraction pattern it is compared to JCPDS cards. The structural properties are greatly influenced by particle size. According to Debay Sherrer equation, which is used to calculate particle size, crystal size is inversely proportional to peak width. So the small crystallite size is related to peak broadening in XRD analysis. The Debay sherrer equation is used to calculate particle size.

$$t = \frac{0.9\,\lambda}{\beta\, cos\theta}$$

λ represents the incident X-ray wavelength and θ and β represent diffraction angle and full width half maximum respectively.

3.1.4 X-Ray density

The X-ray diffraction data can be used for the calculation of sample material’s density [49]. If the lattice constant is known for each sample following formula will be used.

$$\rho x = \frac{8M}{Na3}$$

Where ε represents molecular weight of sample, N is the Avogadro’s number ($6.03x10^{23}$) and "a" is the lattice constant. Eight formula units are possessed by each cell.

3.1.5 Bulk density

The intrinsic properties of materials define the bulk density or measured density. The density formula is generally used for the density calculation.

$$\rho_m = \frac{m}{\pi r2h}$$

Where m represents the mass, r represents the radius; h is the thickness of the pressed pellet sample. For the calculation of measured density, a circular pallet of mass "m" is made using hydraulic press. Vernier caliper is used for measuring thickness and radius of pallet and analytical balance is used for measuring mass of the pallet. The measured parameters are substituted in equation for the resultant density calculation.

3.1.6 Porosity fraction

Along with the alternation in compositions, the increase in the porosity fraction is observed. Following formula is used for calculation of porosity fraction.

$$\boldsymbol{Porosity\ Fraction\ =\ I\ -\ \frac{\rho m}{\rho x}}$$

3.2 Scanning electron microscopy

Scanning electron microscopy is an imaging technique which makes use of high energy electron beams for imaging Nano and bulk surfaces. When the highly energetic beam strikes the sample surface it provides following information.

- Composition of the sample.
- Phase mapping
- Topography of the sample.

When the beam hits the surface of material there will be various kind of interactions and signals are emitted as a result of these interactions such as transmitted electrons, back scattered electrons, secondary electrons, cathodoluminiscence and characteristic X-rays [45].

3.2.1 Basic principle of SEM

When a specimen is irradiated with high energy electron beam, interactions between the incident electrons and the constituent atoms in the specimen produce various signals, as shown in the following figure.[50]

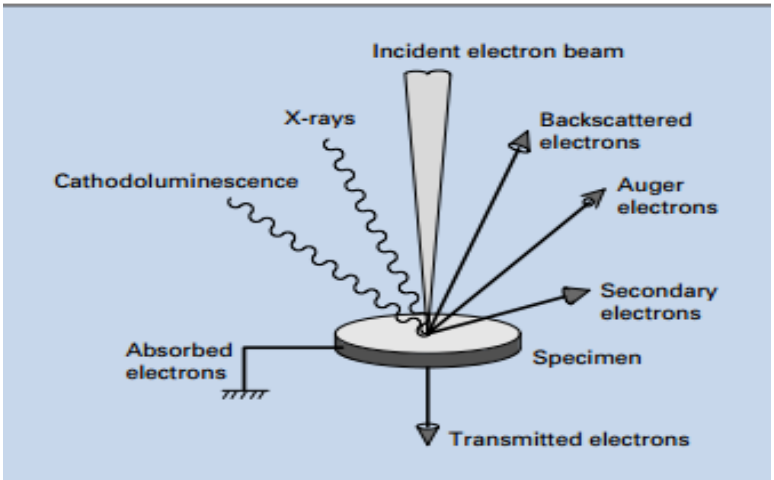

Figure 3.2- Emission of various electrons and EM waves from the specimen.[50]

Electron-matter interactions can be divided into two classes:

1. **Elastic scattering** – the electron trajectory within the specimen changes, but its kinetic energy and velocity remains essentially constant. The result is generation of backscattered electrons (BSE).
2. **Inelastic scattering**– the incident electron trajectory is only slightly changed, but the change in energy results is the generation of different radiations i.e
    - Phonon excitation (heating)
    - Cathodoluminescence (visible light fluorescence)
    - Characteristic x-ray radiation
    - Secondary electrons
    - Auger electrons (ejection of outer shell electrons)

3.2.2 Preparation of SEM samples

SEM is used for the study of surface morphology and for getting 3D images of surface. A very small amount of powdered material was dispersed in water using ultrasonicator for about one hour and then drop of the mixture dripped onto a clean substrate. On substrate surface powder particles are dried and dispersed for further processed of analysis by SEM.

3.3 Fourier transform infrared spectroscopy

The absorption, emission spectra's, Raman scattering and photoconductivity of the material can be obtained by using this analytical technique. The stretching modes of the elements present in composite and chemical purity of the sample can be determined using FTIR. It is known as FTIR because it involves the Fourier, a mathematical term. It collects the data from spectrum of matter. FTIR is used to determine the amount of light that a sample absorbs at a specific wavelength.

3.3.1 Working principle of FTIR

In FTIR, an infrared light beam from a source which is polychromatic is made to fall on splitters. Half portion of the incident light is refracted towards fixed mirror and other half of the incident light is transmitted through a moving mirror. Transmitted light pass through the sample. The information about molecular component and structure of the sample can be obtained by interaction of light with sample. [51]

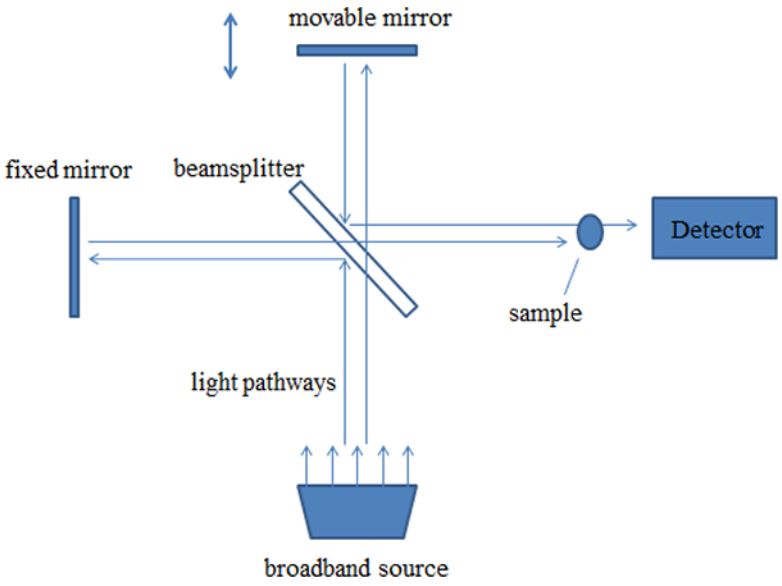

Figure 3.3: Schematic diagram of working principal of FTIR[52]

3.3.2 Applications of FTIR

A gas chromatograph is used to separate the components of a mixture

- The analysis of liquid chromatography fraction can be done using FTIR.

- Tiny samples can be checked with the help of infrared microscope in sample chamber.
- The sample acquiring emitted spectrum of light is obtained FTIR instead of light spectrum through the sample.

3.3.3 Preparation of FTIR samples

KBr pellet method was for sample preparation because alkali salts gives no absorption in IR spectrum. "Potassium salt (KBr) was placed in oven at 100 ^{o}C for one hour for removal of moisture. Small amount of sample and KBr was taken and ground to fine powder and pellet was prepared using pellet die set and Hydraulic press. Mixture of ground KBr and sample was added into the die and it was then placed into the press and with a pumping movement, moved the hydraulic pump handle downward until it shows 3 tons on the scale. Waited for 45 seconds, pressure was released and die was taken out. Finally, a thin sample pellet having thickness in the range of 2-3 mm and diameter of ~13 mm was obtained.

3.4 Electrical properties

3.4.1 Dielectric properties

The LCR meter bridge is used for determination of dielectric properties such as dielectric loss, dielectric constant etc. Firstly the capacitance of pallets were find out using LCR meter then following formula is used for the calculations of dielectric constant.

$$\epsilon^{'} = \frac{Cd}{A\epsilon o}$$

Where C represents the capacitance of the pellet (farad), t represents the thickness of the pellet (Meters), A represents the cross-sectional area of the flat surface of the pellet and ε_0 is the constant of permittivity for free space and its value is equal to 8.85x10-12 F/m. The imaginary part that corresponds to the energy dissipation losses is calculated by using the following equation:

$$\acute{\varepsilon}'' = \acute{\varepsilon} * \boldsymbol{D}$$

There will be some power losses in dielectric materials. These losses are due to the work done in order to overcome frictional and damping forces faced by dipoles during their rotatory motion. The dielectric loss tangent can be found out by using following equation.

$$\boldsymbol{tan\,\delta = D = \frac{\varepsilon''}{\varepsilon'}}$$

Following equation is used for calculation of AC conductivity:

$$\boldsymbol{\sigma_{ac} = \omega \varepsilon \varepsilon_{\circ} tan\delta}$$

3.4.2 AC impedance spectroscopy

The AC impedance parameters of the samples were measured at room temperature. Resistance (R) and reactance (X) were measured over the frequency range of range of 100 Hz to 5 MHz. The impedance is a complex quantity where resistance (R) and reactance (X) shows the real and imaginary parts of impedance in the circuit by the relation:

$$\boldsymbol{Z = R + jX}$$

The impedance -Cole plot shows the resistive behavior of the material. The SI unit of impedance is 'Ω' where resistance (R) and reactance (X) shows the real and imaginary parts of impedance in the circuit by the relation:

$$\boldsymbol{Z' = R = |Z| cos\theta z}$$

$$\boldsymbol{Z" = X = |Z| sin\theta z}$$

The impedance shows the resistive behavior of the material. The SI unit of impedance is 'Ω'. The Cole-Cole plot based on real and imaginary parts of impedance shows contribution of resistance in the material.

3.4.3 Preparation of samples for measurement of electrical properties

For measurement of electrical properties of samples, pellet of each sample was prepared pellet was prepared using pellet die set and Hydraulic press. Each sample was finely grinded before sample preparation. Pellets were prepared using 1 gram of each. Pellets prepared were measured using vernier caliper and found almost same thickness and diameter (2 mm thickness and about 10 mm diameter) for all pellets. By the use of hydraulic press for applying a load of 4 tons for 2 minutes on each pellet. The prepared pellets were kept at 500^{o}C to be sintered for 2 hrs and used for measuring electrical properties" (Dielectric constant & Dielectric loss).

Chapter 4

Results and Discussions

4.1 X-ray diffraction (XRD) results

The room temperature Powder X-Ray Diffraction analysis of the $Mg_{(1-2x)}$ (Co Ni)$_x$ Fe_2O_4 are shown in figure 4.1below, where x= 0.0, 0.05, 0.1, 0.15, 0.20, 0.25. The figure shows well defined sharp diffraction peaks of single phase spinel structure. The peaks shown in the pattern matched well with the (JCPDS NO. 01-88-1940).

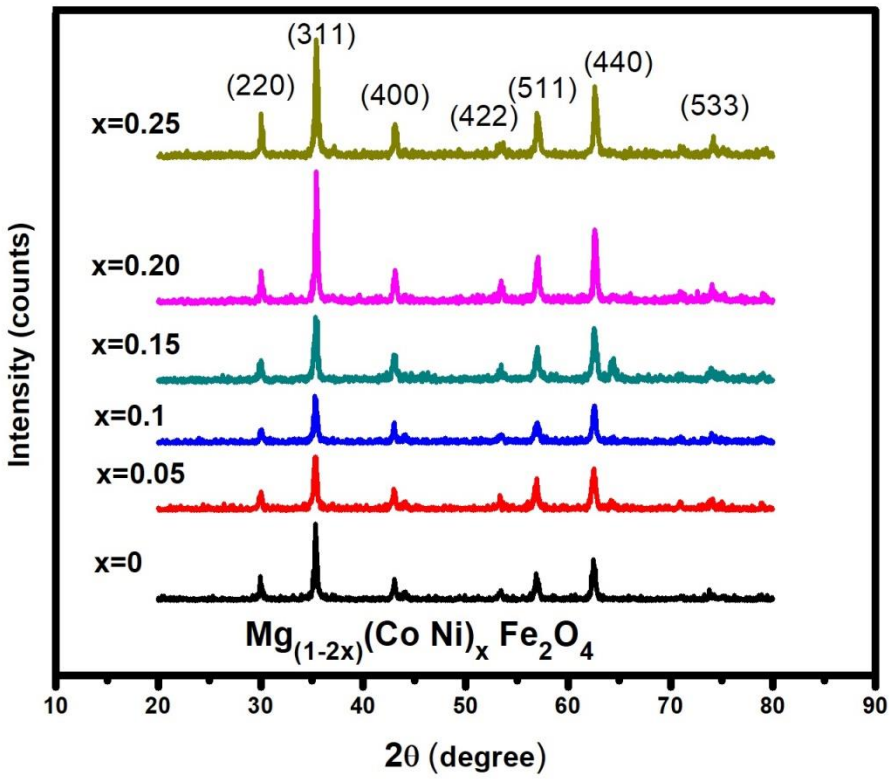

Figure 4.1: XRD patterns of Mg Ferrites with increasing (Ni and Co) concentration.

All samples were calcinated at 800^{o}C for 5 hours before doing the X-Ray Diffraction analysis of the ferrite powder and the results of the diffraction patterns of planes (220),

(311), (400), (422), (511), (440), (533) showed the pure crystalline closed packed face centered cubic arrangement with fd-3m space group [53]. This pattern has no extra peaks such as α-Fe_2O_3.The estimation of crystallite size was done by using the broadening of (311) peak and Debye- Scherrer's equation [54] described as

$$\boldsymbol{D_{hkl} = \frac{0.94\lambda}{\beta_{hkl} cos\theta_{hkl}}}$$

where λ is a wavelength of used x ray (1.54060Å for Cukα), β is FWHM of line broadening, and θ represents the angle of diffraction from respective (hkl). Estimation of lattice parameters has been done using the following formula

$$\boldsymbol{a = \sqrt{d^2(h^2 + k^2 + l^2)}.}$$

The average crystallite size was calculated to be in the range of (~ 50nm to ~66nm). While the lattice parameter and crystallite shown a nonlinear behavior with the substitution of cobalt and nickel ion shown in figure 4.2. Co^{+2} (0.74Å), which has a ionic radii greater than Mg^{+2} (0.72Å) and Ni^{+2} (0.69 Å) which has a smaller ionic radii than Mg^{+2} (0.72Å)[55]. From the literature review it has been seen whenever substitution of element with greater ionic radii has been done an increase in lattice constant and crystallite size is observed and vice versa [55, 56]. So it can be assumed that replacement of Mg^{+2} at the octahedral site by Ni^{+2} causes the reduction of the unit cell [57], resulting in larger lattice constants while replacement of Fe^{+3} (0.645Å) ions from octahedral site by Co^{+2} ions causing the expansion of unit cell, that's why is a nonlinear variation in lattice parameter has been shown in the figure 4.2. Vagerd's law is also used to explain the relation of (Co^{+2}, Ni^{+2}) substitution and lattice constant[58].

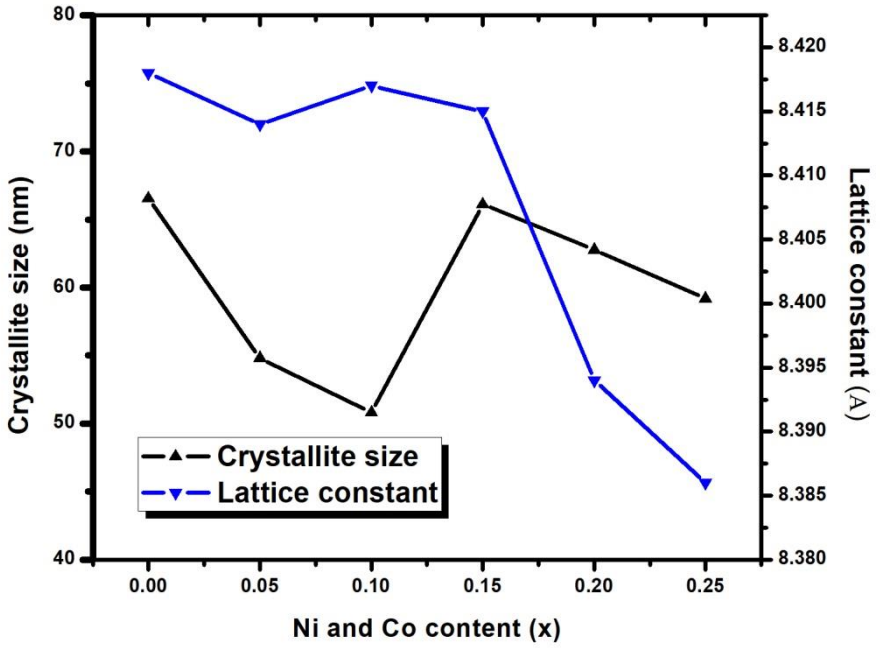

Figure 4.2: Crystallite Size and lattice constant as a function of increasing (Co, Ni) concentration.

Figure 4.3 shows the trend of bulk density and X ray density with increase in the concentration of cobalt and nickel. X ray density is calculated using formula

$$d_x = \frac{8M}{Na^3}$$

Where M represents the molecular weight, N represents the Avogadro's number and a (Å) represents the values of lattice parameter.

From figure 4.3 it is observed that x ray density exhibit the increasing trend with increasing Co^{+2} and Ni^{+2} concentration .As the atomic weight of Ni (58.69amu) and Co (58.93amu) is greater than the Mg (25.31 amu) that's why substitution of Co and Ni leads to increase in the x ray density. we can also assume that as the density of Mg (1.74 g/cm^3) is smaller than that of Ni (8.91g/cm^3) and Co (8.90 g/cm^3) as well as the concentration of atoms in unit volume is Mg is lesser than that of Co and Ni that's why we exhibit increasing trend in x ray density. The bulk density is lower than x ray density. This is because of the existence of pores which are developed during sample preparation or sintering process.

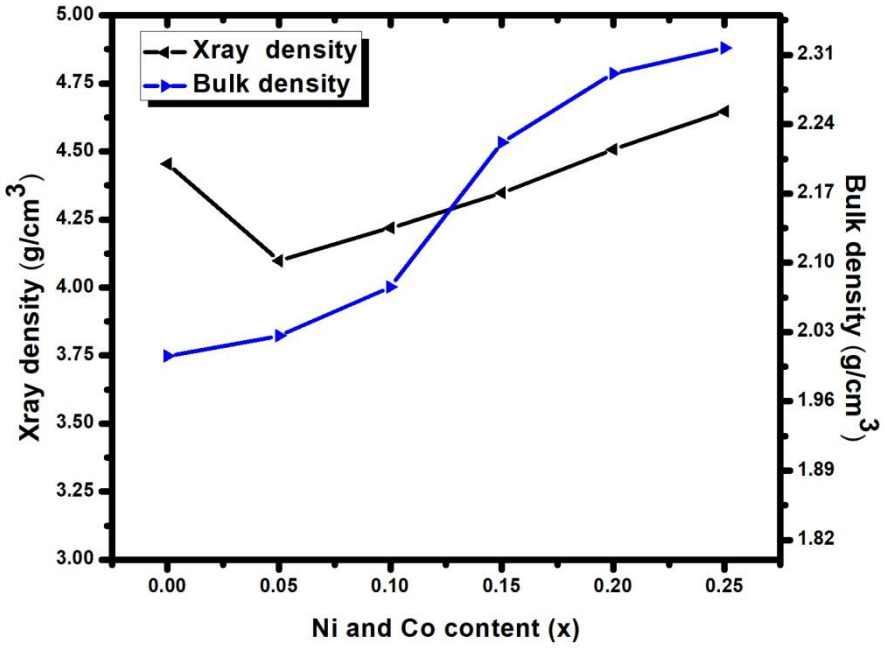

Figure 4.3: Bulk Density and x ray density as a function of increasing (Co, Ni) concentration

Specific surface area of the sample can be calculated using the average crystallite size and bulk density from following relation[59]

$$\boldsymbol{S = \frac{6000}{Dd_B}}$$

Here S is surface area which varies from 51.57 m^2/g to 44.6 m^2/g. while D represents average crystallite size and d_B represents bulk density. The percentage of porosity is also calculated using formula

$$\boldsymbol{P = \left(1 - \frac{d_x}{d_B}\right) X\ 100}$$

Here dx represents the x ray density which decreased from 55 to 49 with increasing Co and Ni concentration.

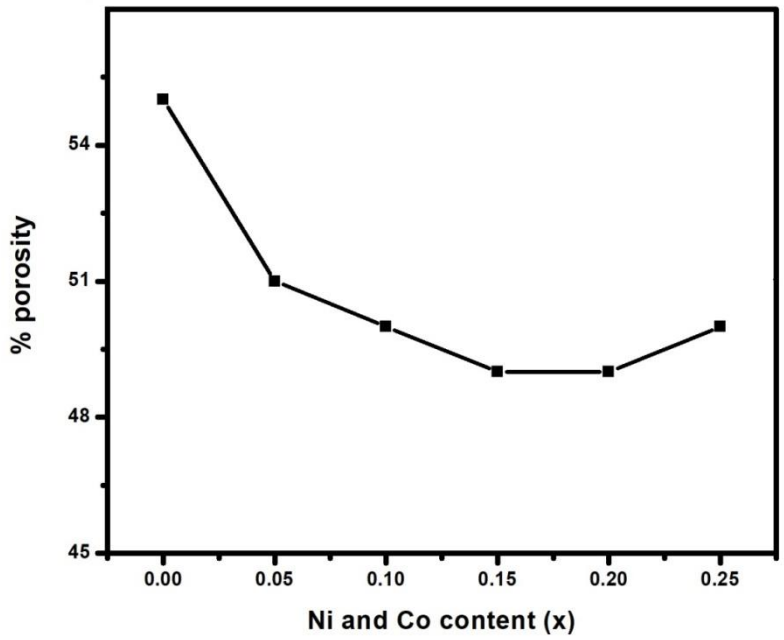

Figure 4.4: % porosity as a function of increasing (Co, Ni) concentration

Table 4.1: Shows the variation of Crystallite size, Lattice constant, X-ray density, Bulk density and Porosity with the increase in (Co, Ni) concentration.

Co and Ni content	Crystallite size (nm)	Lattice constant(Å)	X-ray density(g/cm3)	Bulk density(g/cm3)	Porosity fraction
0.0	66	8.418	4.45	2.00	55
0.05	54	8.414	4.09	2.02	51
0.10	50	8.417	4.21	2.07	50
0.15	66	8.415	4.34	2.22	49
0.20	62	8.394	4.50	2.29	49
0.25	59	8.386	4.64	2.31	50

4.2 Scanning electron microscopy (SEM) analysis

Scanning electron was used to find out the size and morphology of prepared samples. The results are shown in figure 4.5. The results include SEM images of pure magnesium ferrite nanoparticles and cobalt and nickel substituted magnesium ferrites nanoparticles for their different concentrations. For SEM analysis samples were prepared by making their suspension in deionized water using sonication for more than 3 hours. It was revealed that all compositions showed uniform distribution of spherical shape nanoparticles. Particles were separated and distinguish from each other. Little agglomeration was also observed in some compositions. The reason for the agglomeration could be the poor sonication.

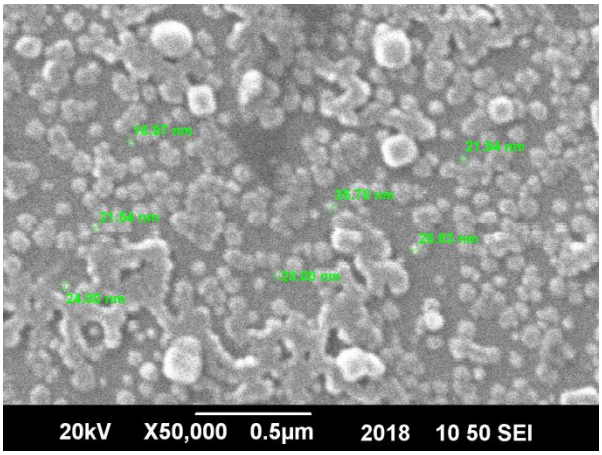

Figure 4.5: SEM image of $MgFe_2O_4$ nanoparticles

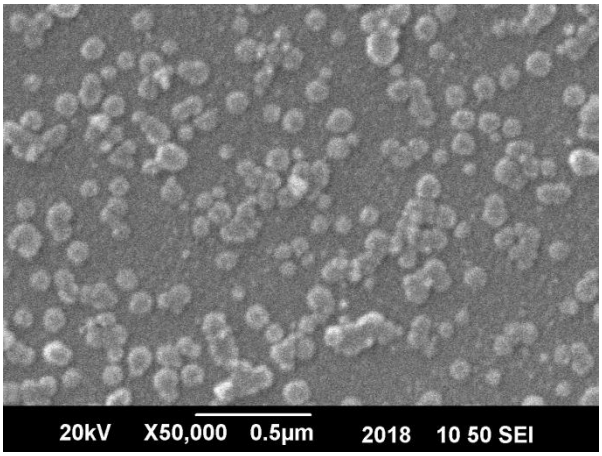

Figure 4.6: SEM image of $MgFe_2O_4$ nanoparticles with Nickel and Cobalt content (x=0.1)

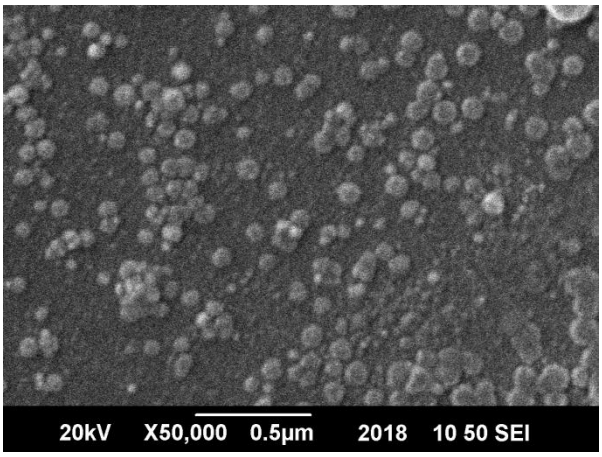

Figure 4.7: SEM image of $MgFe_2O_4$ nanoparticles with Nickel and Cobalt content (x=0.2)

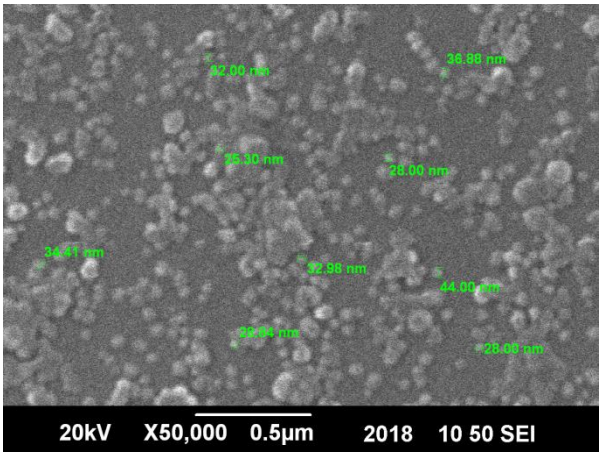

Figure 4.8: SEM image of $MgFe_2O_4$ nanoparticles with Nickel and Cobalt content (x=0.25)

4.3 FT-IR Spectroscopy

The FTIR spectroscopic analysis of $Mg_{(1-2x)}$ (Co Ni)$_x$ Fe_2O_4 are shown in figure 4.9 below, where (x= 0.0, 0.05, 0.1, 0.15, 0.20, 0.2). It was done using kBr pallet in normal room conditions at frequency range of 350 cm^{-1} to 4000 cm^{-1} . The appearance of the two distinct band ν_1 and ν_2 reveals the formation of single phase spinal ferrites. The bands appearing at the higher wavenumbers (ν_1= 563.04 cm^{-1}, 574.52 cm^{-1}) are assigned to tetrahedral (A–site) complexes of Metal and Oxygen, while the frequency bands appearing at lower wavenumbers (ν_2 = 418.10 cm^{-1} , 425.56cm^{-1}) are assigned to octahedral complexes (B-site) of Metal and Oxygen[60]. The variation in ν_1 and ν_2 also

attributed to the changes in bond length of Metal and Oxygen .The tetrahedral vibrational mode is usually higher in frequency than that of octahedral mode due to its longer bond length of each cluster. The ν_1 and ν_2 absorption bands are also assigned as metal-oxygen stretching vibration mode at A and B sites. In figure change in the (ν_1, ν_2) can be attributed to the tendency of (Co, Ni) ions to occupy both A and B sites as well as decrease in a bond length.

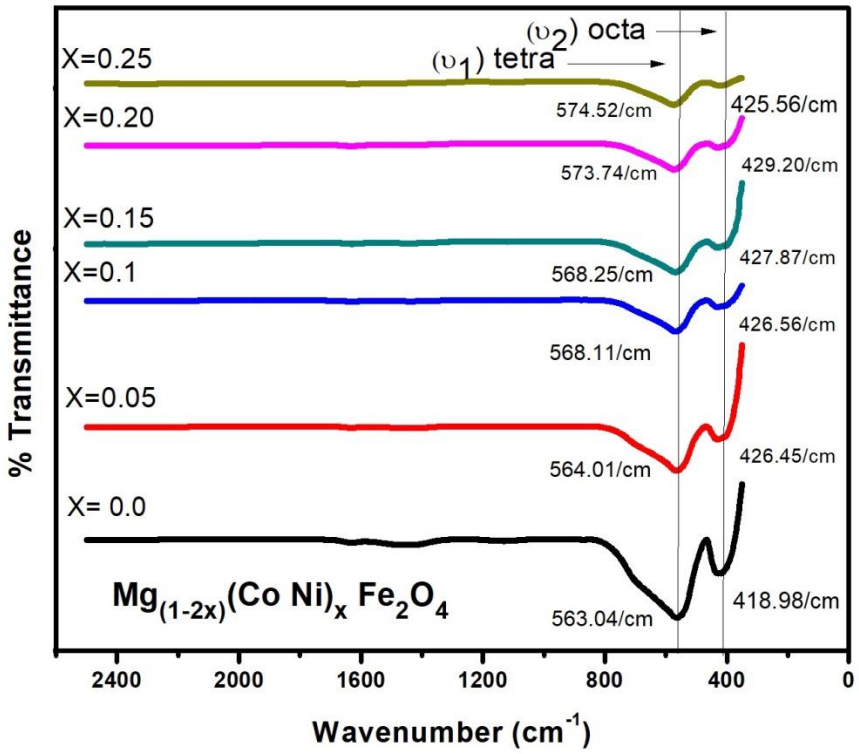

Figure 4.9: FTIR spectra of Mg Ferrites with increasing (Ni and Co) concentration.

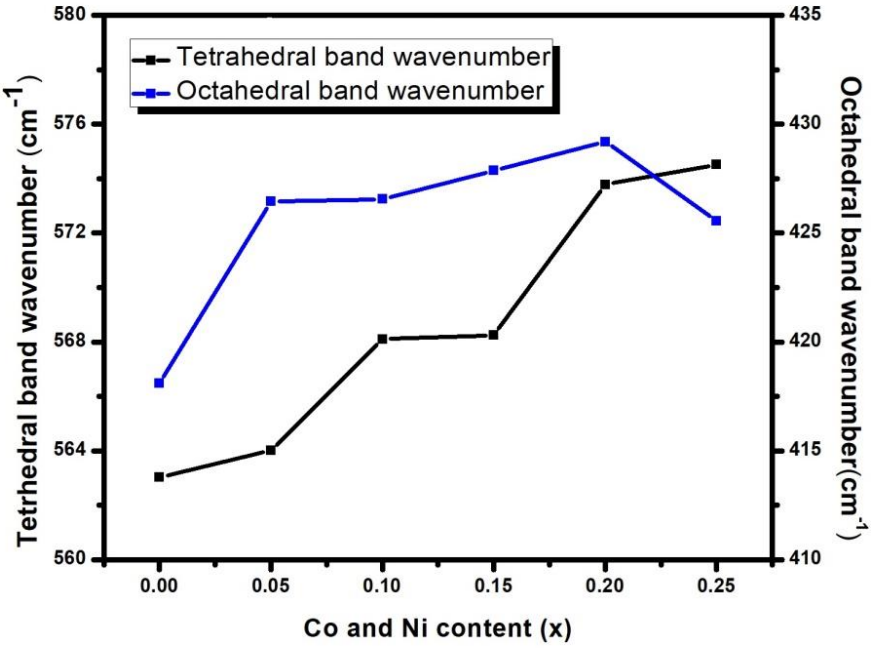

Figure 4.10: Variation at A and B site with changing (Co, Ni) concentration.

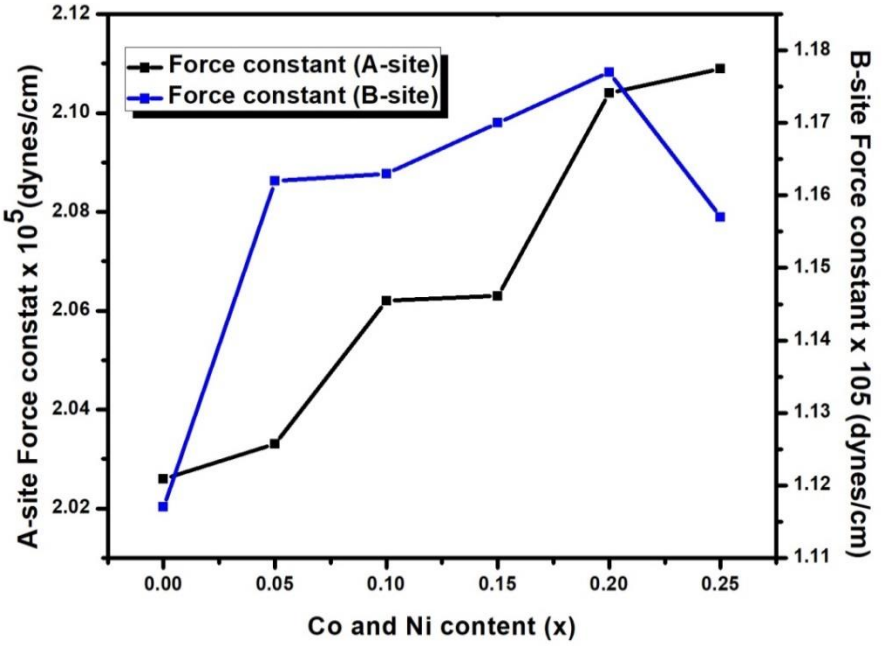

Figure 4.11: Variation of Force constant at A and B site with (Co, Ni) concentration

4.4 Dielectric constant

Permittivity is an ability of a material to polarize in an electric field. The Dielectric parameters were calculated using LCR meter in a frequency range from 100 HZ-10^3HZ. The pelletized samples of average diameter 13mm and average thickness of 2mm were prepared. Dielectric permittivity can be described as

$$\varepsilon_r = \varepsilon' + i\varepsilon''$$

Where ε_r represents dielectric permittivity of a medium, ε' and ε'' are the real and imaginary parts of it. The storage of electromagnetic energy (EM) is represented by the real part known as dielectric constant, whereas the thermal conversion is attributed to the imaginary part known as dielectric loss. The main reason for the dielectric loss is the lag of response of dielectric material to the applied electric field. Dielectric constant can be calculated using formula

$$\varepsilon' = Ct/\varepsilon_0 A$$

Where C is the capacitance which is calculated using LCR meter, t is the thickness and A is the area of pallet used. The dielectric properties of $Mg_{(1-2x)}(Co\ Ni)_x Fe_2O_4$ are, where (x= 0.0, 0.05, 0.1, 0.15, 0.20, 0.2) are calculated and the effect of increasing frequency has been studied.

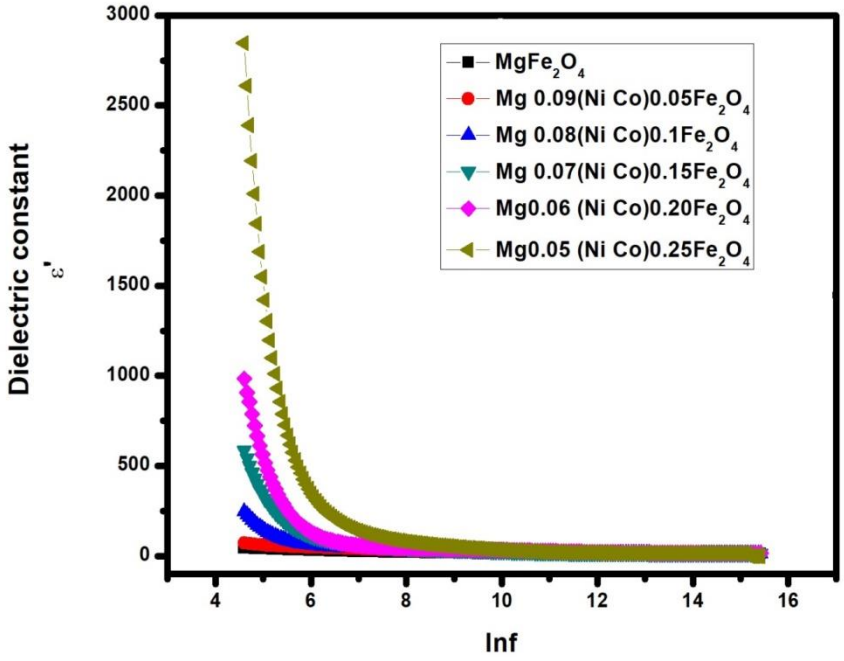

Figure 4.12: Variation of dielectric constant with frequency

In figure 4.12 as frequency increase a decreasing trend in dielectric constant values can be seen which becomes constant at higher values of frequency. It is a normal dielectric dispersion which can be narrated by the Maxell- Wagner type interfacial polarization [61], In any material interfacial, ionic , electronic and dipolar polarizations contributes to the dielectric constant. Dipolar and interfacial polarizations are significant at low frequencies while at high frequencies electronic polarization paly more vital role towards dielectric constant[62].The high values of the dielectric constant can also be correlated with the space charge polarization mechanism. In this mechanism the conductivity of grain boundaries have high resistance which differs from that of grains having low resistance, hence the charge carriers face different resistances causing an accumulation of charges at separating boundaries which in turn produces an increase in the dielectric constant. At lower frequencies charge carrier provides fast response to the variation in electric field while at higher frequencies response of charge carriers is very slow , that responses then contribute to polarization and then to dielectric constant.

In our samples increase in the cobalt and nickel doping also increase the dielectric constant value. Pure magnesium ferrite sample has dielectric constant of 43 as reported earlier [63] while with every rise of doping the increase in the dielectric value is very significant, for (Co, Ni) value 0.25 it risen up to 2846. As Co+2 ions can occupy both tetrahedral and octahedral sites which emerges competition between Fe^{+3} and Mg^{+2} ions for occupying tetrahedral and octahedral position[64]. While Ni^{+2} prefer to occupy octahedral sites which also effect the distribution of Fe^{+2}/Fe^{+3} at octahedral site and ultimately increase in the hopping of electrons[38].So we can say due to the occupation of cobalt and nickel ions at both octahedral and tetrahedral sites the migration of electron between Fe^{+2} and Fe^{+3} increases which in results increases the dielectric constant.

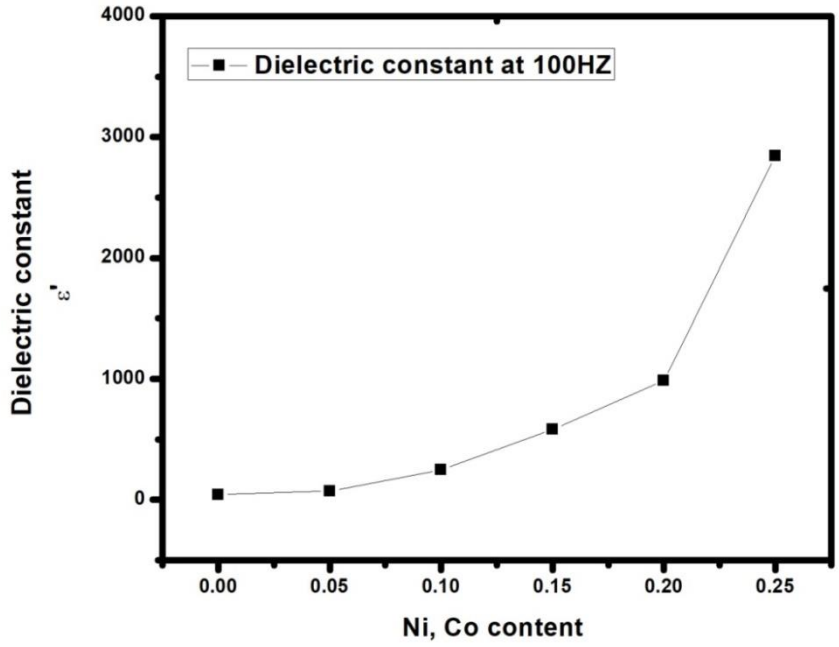

Figure 4.13: Dielectric constant at 100HZ for increasing (Co, Ni) concentration.

4.5 Dielectric loss

Dielectric loss is an imaginary part of a permittivity which deals with the energy loss.it can be represented as $\varepsilon'' = \varepsilon' \tan\delta$. There are many factors which affect the dielectric loss factor, which includes crystal lattice, impurities and defects etc. In figure 4.14 variation of dielectric loss with frequency can be seen. It is clearly shown that with increasing

frequency the value of dielectric constant decreases exponentially for all samples and then become constant at higher frequencies.

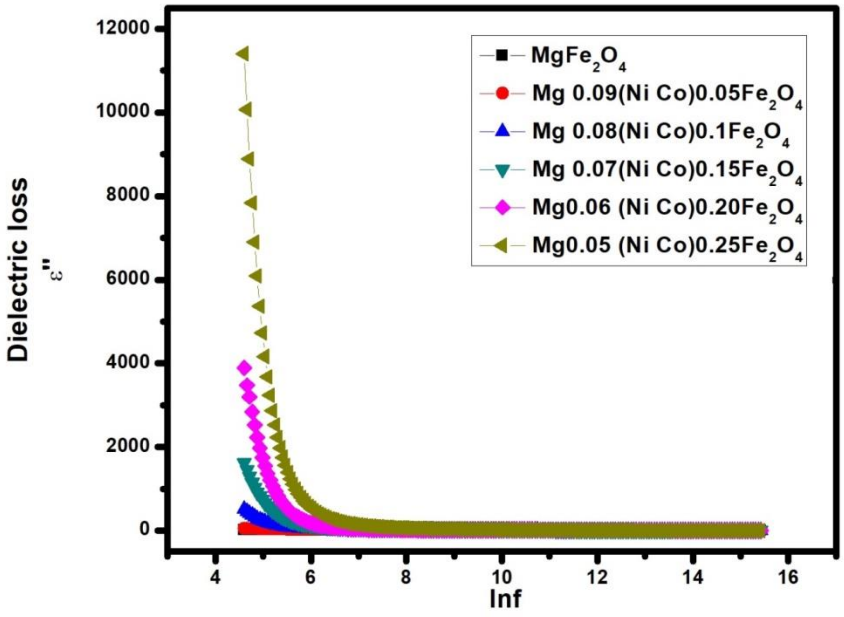

Figure 4.14: Variance of dielectric loss with frequency

At lower frequency the value of dielectric loss is higher which is 20 for magnesium ferrite sample and then increased to 11410 for sample doped with cobalt and nickel (0.25) concentration. According to Koop's theory at low frequency grain boundaries provides high resistance so dielectric losses are more but at high frequencies grain boundaries resistance decreased and beyond certain value of frequency exchange of hopping electrons can't follow the alternating field which results in a constant dielectric loss value[65]. As by increasing the concentration of nickel and cobalt ions the grain boundry resistance also increased due to greater grain size.

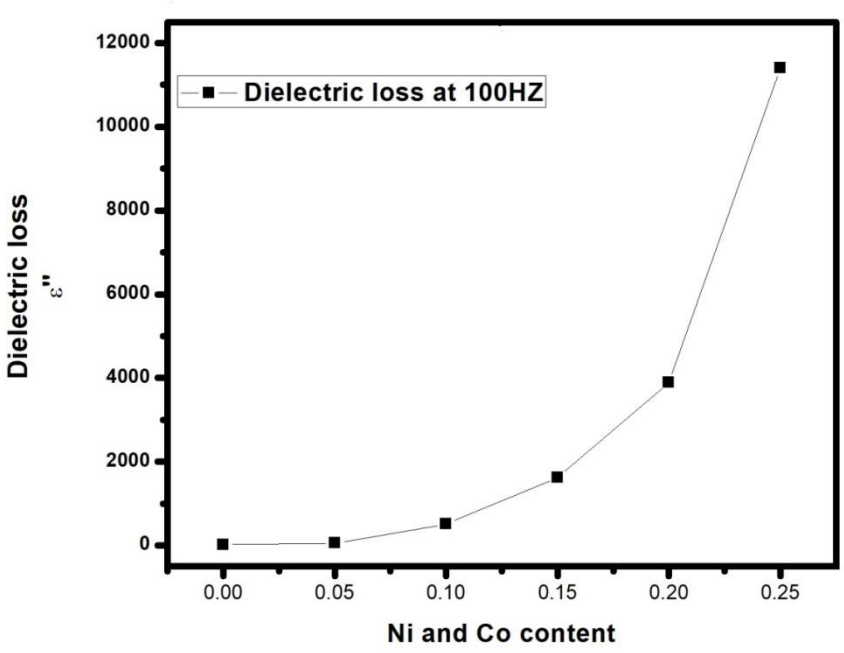

Figure 4.15: Dielectric loss at 100HZ for increasing (Ni ,Co) concentrations

4.6 Dielectric tangent loss

Dielectric tangent loss is a ration of dielectric constant and dielectric loss. It can also calculated using following formula[40]

$$\tan\delta = \frac{1}{\omega \varepsilon_o \rho}$$

where ω=2πf, f is a frequency of applied field, ε_o is a permittivity of free space and ρ is a resistivity. The tangent loss value also decreased with increasing frequency range as shown in figure 4.16 dielectric tangent loss is caused by the lag in polarization with increase of applied electric field.

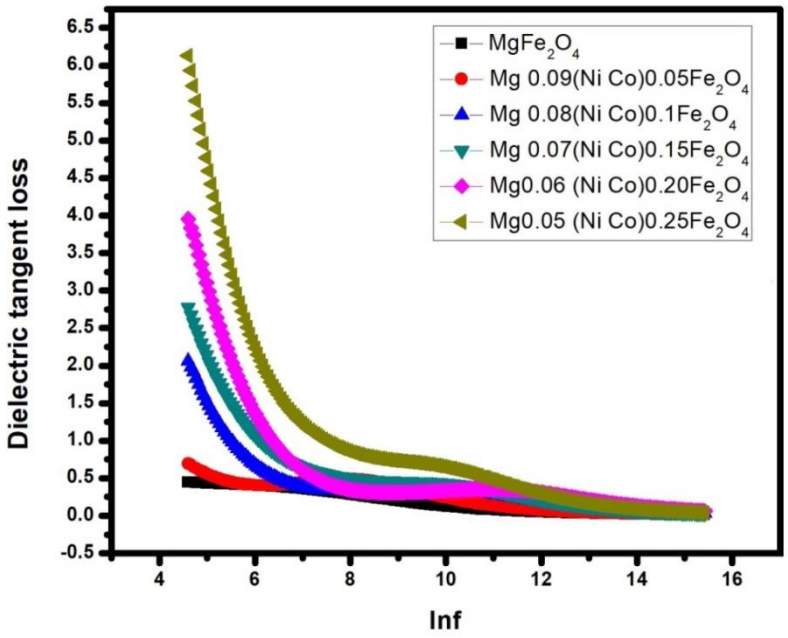

Figure4.16: Variation of tangent loss with frequency

In figure 4.16 compositional effects can be seen on dielectric loss values. By increasing the concentration of nickel and cobalt dielectric tangent loss values has been increased. The reason could be increase in grain size, impurities or imperfections in the crystal lattice.

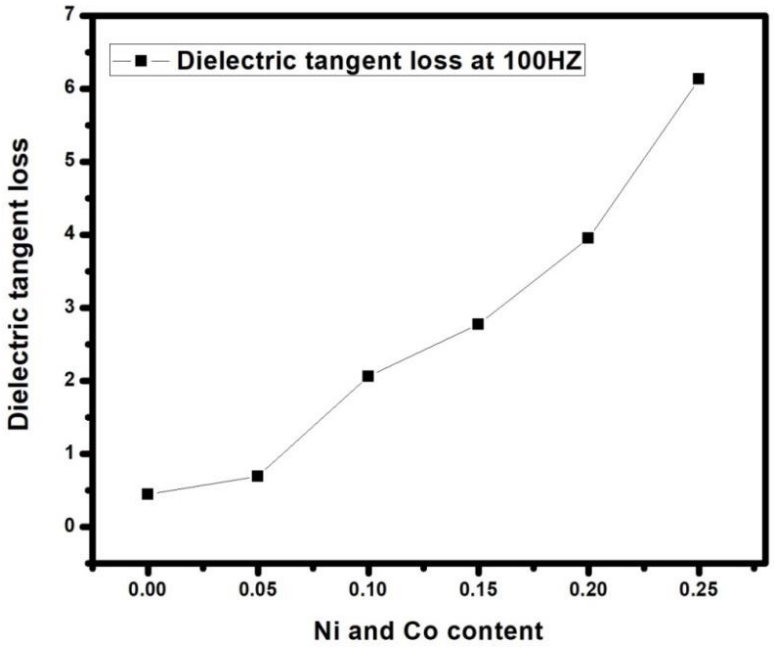

Figure 4.17: Dielectric tangent loss at 100 HZ with increasing (Co, Ni) concentration

4.7 Ac Conductivity

Conductivity is the physical property of a material which characterizes the conducting power inside the material. in spinel ferrites conduction can be described by Verwey mechanism[66].which said that the electrical conductivity in ferrites is mainly due to the hopping of electrons between the ions of the same element presented in more than one valence state at octahedral site[67].

The AC conductivity of all samples were calculated at room temperature using the following formula

$$\sigma_{ac} = \omega \varepsilon_0 \varepsilon''$$

Where $\omega=2\pi f$, f represented the frequency, ε_o represents the permittivity of free space and ε'' represents dielectric[68].

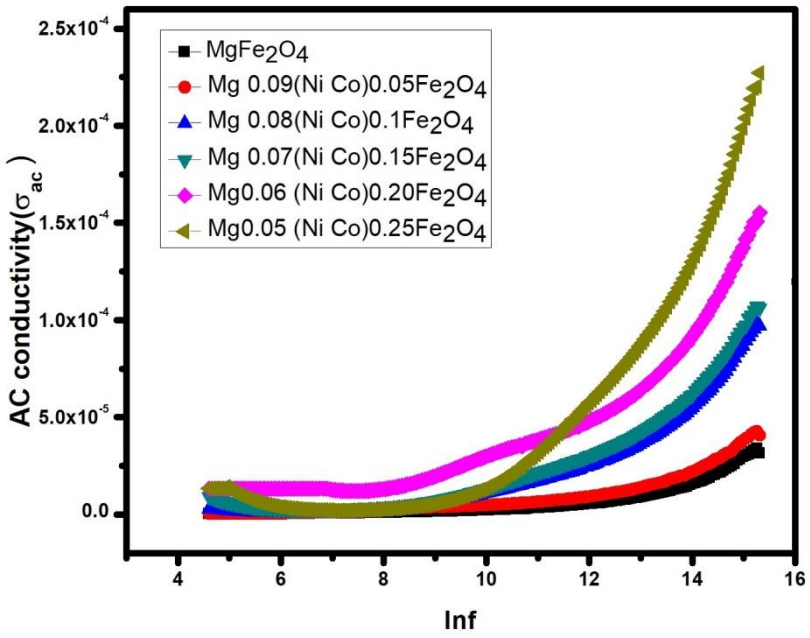

Figure 4.18: Variation of AC conductivity with frequency

According to literature, the total conductivity is by following relation [69]

$$\sigma_{tot} = \sigma_o\,(T) + \sigma(\omega, T) = \sigma_o\,(T) + B\omega^s$$

where $\sigma_o(T)$ represents dc conductivity which is frequency independent and occur due to band conduction. $\sigma(\omega, T)$ represents ac conductivity due to hopping process among ions of same element present in more than one valence state. In above relation, the B and s are constants which depends on both temperature an composition. The trend of the AC conductivity is shown in a figure 4.18. It can be seen that at low frequency range the AC conductivity is independent of the frequency and an increasing trend can be seen with increase in frequency for each the sample. This behavior is in accordance to Maxwell-Wagner type. According to this, at lower frequencies the conductivity is low due to large hindrance at grain boundaries (related to dc conductivity) for the movement of electrons. As the frequency increases, the conductivity across the grain boundaries increases due to the more effective hopping of electrons between Fe^{2+} and Fe^{3+} ions.

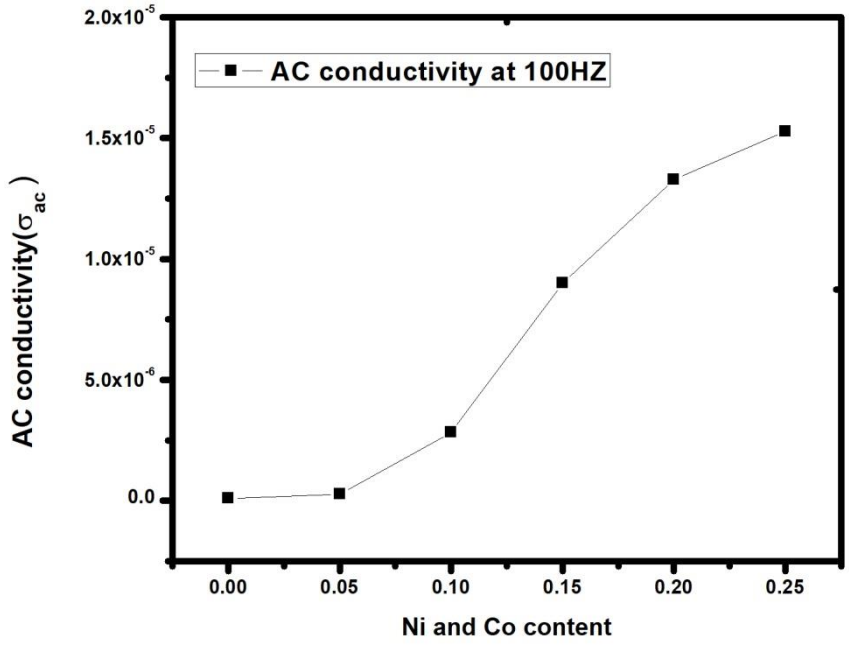

Figure 4.19: AC conductivity at 100HZ for increasing (Ni, Co) concentration

4.8 Ac Impedance

The real and imaginary parts of impedance of samples were calculated in response to frequency at room temperature in figure 4.20 and 4.21. The complex analysis of impedance actually describes the detailed analysis of interaction at grain and grain boundaries. Real part depicts frequency dependent variation in resistive while imaginary part depicts the variation in reactive part of the impedance. A decreasing trend of impedance has been seen with increasing cobalt and nickel concentration which indicates increase in conductivity at grain boundaries. The decreasing trend in the impedance with increase in doping refers to increase in conductivity with in accordance to the previously calculated results of dielectric constant. At higher frequencies impedance is becomes constant due to reduction in space charge polarization values. While at lower values of frequencies high values of impedance can be seen due to high space charge polarization[46, 70]. A broad and a-symmetric trend was also seen in imaginary impedance plots with increase in Ni and Co concentration which indicates multiple

relaxations and deviation from Debye behavior. This is a characteristic of semiconductors.

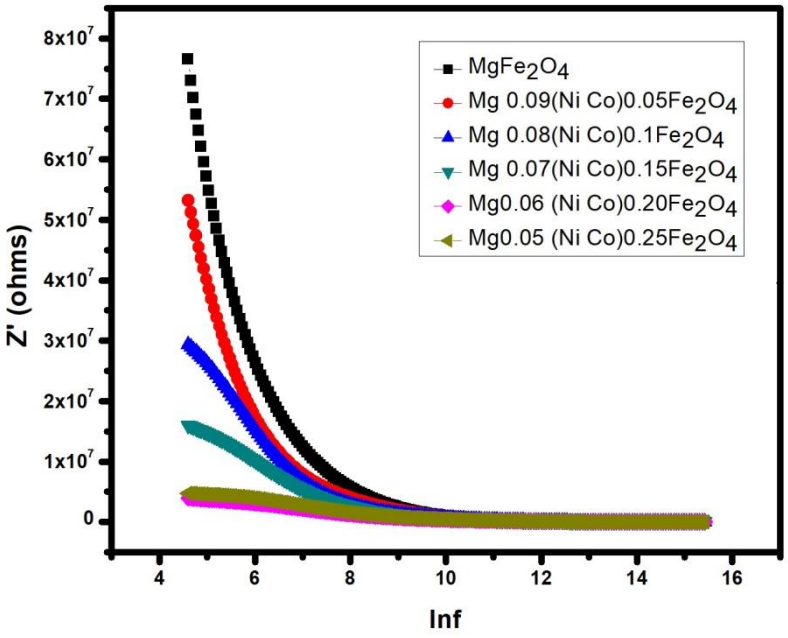

Figure 4.20: Variation of real part of impedance with frequency.

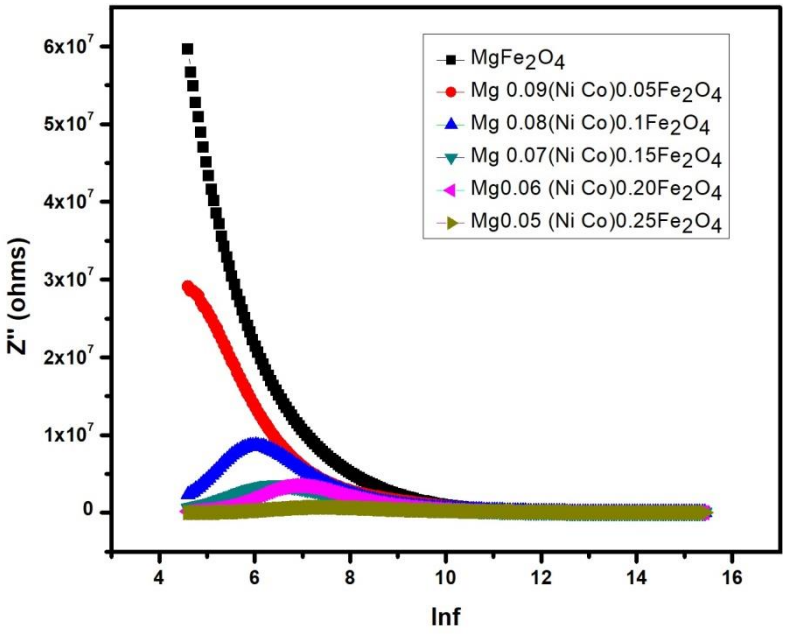

Figure 4.21: Variation of imaginary part of impedance with frequency.

Figure 4.22 shows the Cole-Cole (Z' vs. Z'') plot of magnesium ferrite and its Cobalt and nickel doped samples with concentration (0.05, 0.1, 0.15, 0.20, 0.25). Semi curved lines are shown of each composition at different frequencies. Using Cole-Cole plot analysis we can differentiate the resistance effect of intrinsic of grain, grain boundaries, sample-electrode effect, defects, and relaxation process etc. Appearance of semicircle in the plot represents a relaxation process, and radius of semicircle measures the resistance of the sample whose center lies on the Z' axis, if the conduction is of Debye type. For a non-Debye type conduction process, a depressed semicircle always appears. Usually For the Cole-Cole plot three distinct semicircles appears in the plot, the semicircle appears at low frequency range assigned to grain boundaries resistance, mostly grains boundaries has more resistance than the grain bulk because of the more structural and chemical defects present. So charge carriers at grain boundaries do not follow the variations at low frequency and relax at low frequency range. The semicircle at high frequency zone corresponds to resistive interior grain effect and that of third semicircle is associated to the electrode effect [71]. The decrease in radius the semicircle decreases with increases in Nickel and Cobalt concentration indicating the decrease in resistance of the material [72].

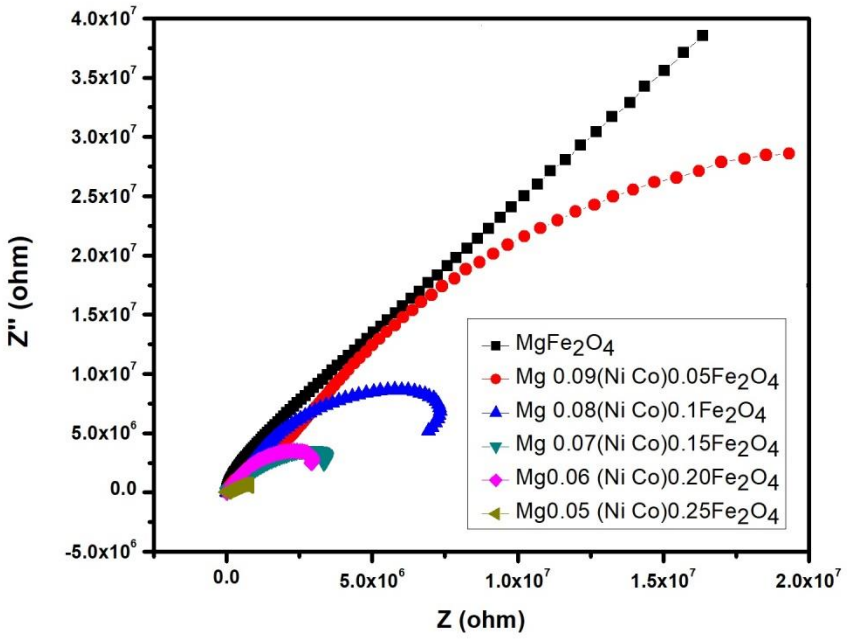

Figure 4.22: Complex impedance spectra of $Mg_{(1-2x)}$ (Co Ni)$_x$ Fe_2O_4 (x= 0.0, 0.05, 0.1, 0.15, 0.20, 0.25)

4.9 Complex Electric modulus

Electric modulus plots can explains the relaxation and conduction behavior of materials. Figure 4.23 and 4.24 shows the frequency dependent real and imaginary part of electric modulus at constant temperature with different compositions of Nickel and Cobalt. In figure 4.23, at lower frequencies M′ values are very small and which represents negligible electrode effect. At higher frequencies sigmoidal increase in the value of M' may be due to the short range mobility of charge carriers. Two different peaks at low and high range frequencies represent that both the grain and grain boundaries resistance playing their roles in the conduction mechanism of the system. In figure 4.24 M″ two distinct peaks representing the grain and grain boundaries effect. This plot also represents a clear shift of relaxation peaks towards higher frequencies with the increase of Nickel and Cobalt content which suggest that in low frequency region charge carriers moving over long distances and attributed to hopping process. And in high

frequency region charge carriers are moving over a short distances correlated with relaxation polarization.[73]

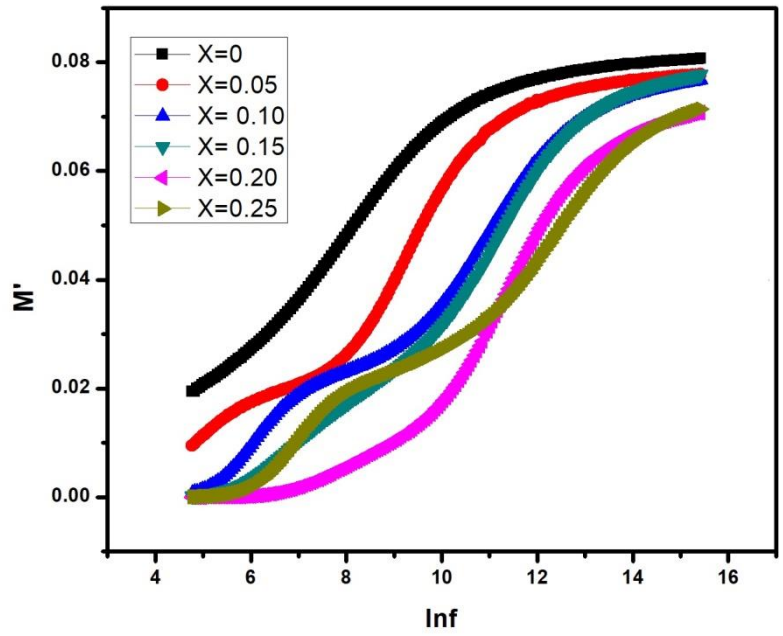

Figure 4.23: Variation of real part of electric modulus with frequency.

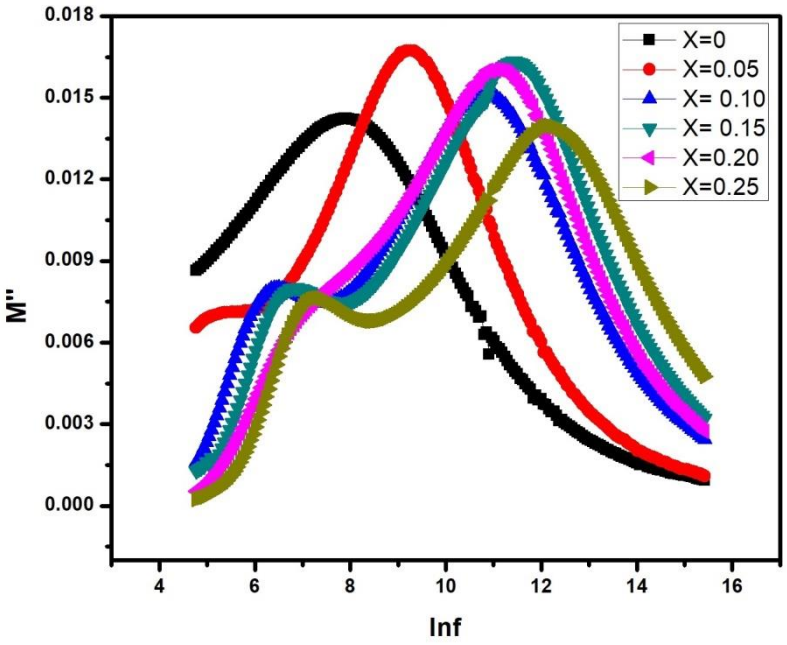

Figure 4.24: Variation of imaginary part of electric modulus with frequency.

Table 4.2: shows the variation of dielectric constant, dielectric loss, tangent loss, AC conductivity, AC impedance at 100HZ

Ni and Co Content	Dielectric Constant at 100HZ	Dielectric Loss at 100HZ	Tan Loss at 100HZ	AC Conductivity at 100HZ	AC impedance at 100 HZ
0.0	43	19	0.4	$1x10^{-7}$	$7.65x10^{7}$
0.05	71	49	0.7	$2.7x10^{-7}$	$5.31x10^{7}$
0.10	247	509	2.0	$2.8x10^{-6}$	$2.93x10^{7}$
0.15	584	1619	2.7	$8.9x10^{-6}$	$1.59x10^{7}$
0.20	983	3887	3.9	$1.3x10^{-5}$	$3.94x10^{6}$
0.25	2846	11410	6.1	$1.2x10^{-5}$	$4.75x10^{6}$

Conclusions

We reported the preparation of $Mg_{(1-2x)}(Co\ Ni)_xFe_2O_4$, x= 0.05, 0.10, 0.15, 0.20, 0.25 by sol gel auto-combustion route. The X-ray powder diffraction technique was used to investigate the structure of synthesized samples. The obtained XRD patterns confirmed the formation of close packed face centered cubic arrangement of nanoparticles. No impurity peaks were observed, confirming the purity of the substance. The crystallite size, calculated using the Scherer formula, no definite increasing or decreasing trend in crystallite size value was seen. It was in the range of 50 nm to 66 nm confirming small grain size. The increase in bulk density and X-Ray density was observed which is subjected to the greater density and molecular mass of cobalt ion and nickel ion than that of magnesium ions. Due to these increase in porosity fraction was as seen. FTIR analysis also confirmed the formation of single phase spinal ferrite. Bands in the range of (ν_1= 563.04 cm^{-1}, 574.52 cm^{-1}) and (ν_2 = 418.10 cm^{-1} , 425.56cm^{-1}) represents tetrahedral and octahedral sites respectively. The SEM images confirmed the formation of uniformly distributed spherical ferrite nanoparticles. In the dielectric properties, dielectric constant of samples were increased by increasing the (Co, Ni) content. Meanwhile increase in the the dielectric loss factor was also found by increasing the (Co, Ni) content. The AC conductivity showed that by increasing the (Co, Ni) content in magnesium ferrite value increased but then after certain concentration of (Co, Ni) is starts decreasing, that reflects that at higher concentration hopping mechanism reduced which in results decreased AC conductivity. The experimental route proved to be an efficient, inexpensive and straight forward procedure for the synthesis of ferrite nanoparticles.

Future Work

Such a nanohybrid can absorb electromagnetic spectrum, so the studies of their microwave absorption as well as UV-Vis characterization can relate to important data which can be deployed for military applications. Often, to make the polymer blends somewhat conductive, different metallic media are added using various polymerization techniques. It's only natural that the next step regarding this research would be to add such a nanohybrid in a polymer matrix to study the mechanical as well as microwave properties of such an advanced hybrid. Owing to their enhanced dielectric properties, such a nanohybrid can be used in batteries cathode as well as in the construction of aerospace parts by incorporation of thermoset resins rendering them high stiffness and strength even at very high temperatures.With the advancement in the field of composites and their versatile use in various industries, such a hybrid can revolutionize the field of nanosciences as well as nanotechnology , pushing the boundaries in the real of magnetism , dielectric , optical and electromagnetic application.

References

1. Gul, I., et al., Structural, magnetic and electrical properties of Co1− xZnxFe2O4 synthesized by co-precipitation method. Journal of magnetism and magnetic materials, 2007. **311**(2): p. 494-499.
2. Djurberg, C., et al., Dynamics of an interacting particle system: evidence of critical slowing down. Physical review letters, 1997. **79**(25): p. 5154.
3. Bradford, P., The aggregation of iron oxide nanoparticles in magnetic fields. 2012, University of Birmingham.
4. Iacovacci, V., et al., Magnetic Field-Based Technologies for Lab-on-a-Chip Applications, in Lab-on-a-Chip Fabrication and Application. 2016, InTech.
5. Flinn, R.A.et al. Engineering materials and their applications. Engineering Materials and Their Applications, 4th Edition, by Richard A. Flinn, Paul K. Trojan, pp. 1056. ISBN 0-471-12508-3. Wiley-VCH, December 1994., 1994: p. 1056.
6. Hilpert, S.et al. phsik. Ges, 1909. **11**: p. 293.
7. Snoek, J.et al, Magnetic and electrical properties of the binary systems MO. Fe2O3. Physica, 1936. **3**(6): p. 463-483.
8. Néel, L,et al. Antiferromagnetism and ferrimagnetism. Proceedings of the Physical Society. Section A, 1952. **65**(11): p. 869.
9. Koops, C,et al. On the dispersion of resistivity and dielectric constant of some semiconductors at audiofrequencies. Physical Review, 1951. **83**(1): p. 121.
10. Chen, C.-W,et al. Magnetism and metallurgy of soft magnetic materials. 2013: Courier Corporation.
11. Yeadon, W.H.et al., Handbook of small electric motors. Vol. 1040. 2001: McGraw-Hill New York.
12. Bragg, W.H,et al. The structure of the spinel group of crystals. The London, Edinburgh, and Dublin Philosophical Magazine and Journal of Science, 1915. **30**(176): p. 305-315.

13. Gorter, E.W,et al. Saturation magnetization and crystal chemistry of ferrimagnetic oxides. I. II. Theory of ferrimagnetism. Philips Res. Rep., 1954. **9**: p. 295-320,321-365.
14. Clarricoats,et al. Microwave ferrites. 1961: Wiley.
15. Barth, T.F,et al. Spinel structures: with and without variate atom equipoints. Zeitschrift für Kristallographie-Crystalline Materials, 1932. **82**(1-6): p. 325-341.
16. Mathew, D.S. and R.-S. Juang, An overview of the structure and magnetism of spinel ferrite nanoparticles and their synthesis in microemulsions. Chemical Engineering Journal, 2007. **129**(1): p. 51-65.
17. Gomes, J., et al., Rietveld structure refinement of the cation distribution in ferrite fine particles studied by X-ray powder diffraction. Journal of magnetism and magnetic materials, 2005. **289**: p. 184-187.
18. Mittal, V., et al., Cation distribution in NixMg1− xFe2O4 studied by XPS and Mössbauer spectroscopy. Solid state communications, 2006. **137**(1-2): p. 6-10.
19. Amer, M., et al., Mössbauer, Infrared and X-ray Studies for Ni_ {0.5} Zn_ {0.5} Cr_xFe_ {2-x} O_4 Ferrites. Turkish Journal of Physics, 2005. **29**(3): p. 163-177.
20. Brockhouse, B., BN Brockhouse, LM Corliss, and JM Hastings, Phys. Rev. 98, 1721 (1955). Phys. Rev., 1955. **98**: p. 1721.
21. Nalbandian, L., et al., Hydrothermally prepared nanocrystalline Mn–Zn ferrites: synthesis and characterization. Microporous and Mesoporous Materials, 2008. **114**(1-3): p. 465-473.
22. Yáñez-Vilar, S., et al., A simple solvothermal synthesis of MFe2O4 (M= Mn, Co and Ni) nanoparticles. Journal of Solid State Chemistry, 2009. **182**(10): p. 2685-2690.
23. Xia, A. and H. Zhang, Effects of excessive Zn2+ ions on intrinsic magnetic and structural properties of Ni0. 2Zn0. 6Cu0. 2Fe2O4 powder prepared by chemical coprecipitation method. Current Applied Physics, 2010. **10**(3): p. 825-827.
24. Lerouge, F., G. Cerveau, and R.J. Corriu, Supramolecular self-organization in non-crystalline hybrid organic–inorganic nanomaterials induced by van der Waals interactions. New Journal of Chemistry, 2006. **30**(10): p. 1364-1376.

25. Banerjee, A., et al., Catalytic activities of cobalt, nickel and copper ferrospinels for sulfuric acid decomposition: the high temperature step in the sulfur based thermochemical water splitting cycles. international journal of hydrogen energy, 2011. **36**(8): p. 4768-4780.
26. Samoila, P., et al., The effect of chelating/combustion agent on catalytic activity and magnetic properties of Dy doped Ni–Zn ferrite. Materials Chemistry and Physics, 2012. **136**(1): p. 241-246.
27. Druc, A., et al., Optimization of synthesis conditions and the study of magnetic and dielectric properties for MgFe2O4 ferrite. Open Chemistry, 2013. **11**(8): p. 1330-1342.
28. Shirsath, S.E., et al., Chemical tuning of structure formation and combustion process in CoDy 0.1 Fe 1.9 O 4 nanoparticles: influence@ pH. Journal of nanoparticle research, 2013. **15**(10): p. 1976.
29. Sulaiman, N., et al., Superparamagnetic calcium ferrite nanoparticles synthesized using a simple sol-gel method for targeted drug delivery. Bio-medical materials and engineering, 2015. **26**(s1): p. S103-S110.
30. Jeseentharani, V., et al., Synthesis of metal ferrite (MFe2O4, M= Co, Cu, Mg, Ni, Zn) nanoparticles as humidity sensor materials. Journal of Experimental Nanoscience, 2013. **8**(3): p. 358-370.
31. Mouli, K.C., T. Joseph, and K. Ramam, Synthesis and magnetic studies of Co-Ni-Zn ferrite nano crystals. Journal of nanoscience and nanotechnology, 2009. **9**(9): p. 5596-5599.
32. Özgür, Ü., Y. Alivov, and H. Morkoç, Microwave ferrites, part 1: fundamental properties. Journal of materials science: Materials in electronics, 2009. **20**(9): p. 789-834.
33. Gul, I., et al., Physical and magnetic characterization of co-precipitated nanosize Co–Ni ferrites. Scripta Materialia, 2007. **56**(6): p. 497-500.
34. Pradeep, A., P. Priyadharsini, and G. Chandrasekaran, Sol–gel route of synthesis of nanoparticles of MgFe2O4 and XRD, FTIR and VSM study. Journal of Magnetism and Magnetic Materials, 2008. **320**(21): p. 2774-2779.

35. Smitha, T., et al. Electrical and magnetic properties of nano-sized magnesium ferrite. in IOP Conference Series: Materials Science and Engineering. 2015. IOP Publishing.
36. BORTNIC, R.-A., et al., SYNTHESIS OF COBALT FERRITE NANOPARTICLES VIA A SOL-GEL COMBUSTION METHOD. Studia Universitatis Babes-Bolyai, Chemia, 2016. **61**(4).
37. Thankachan, S., et al., A comparative study of structural, electrical and magnetic properties of magnesium ferrite nanoparticles synthesised by sol-gel and co-precipitation techniques. Journal of experimental Nanoscience, 2013. **8**(3): p. 347-357.
38. Moradmard, H., et al., Structural, magnetic and dielectric properties of magnesium doped nickel ferrite nanoparticles. Journal of Alloys and Compounds, 2015. **650**: p. 116-122.
39. Mahalakshmi, S. and K.S. Manja, Ac electrical conductivity and dielectric behavior of nanophase nickel ferrites. Journal of Alloys and Compounds, 2008. **457**(1-2): p. 522-525.
40. Hashim, M., et al., Structural, Dielectric, AC Conductivity, and Magnetic Properties of Cr3+ Substituted Ni–Mg Ferrite Nanoparticles. Journal of Nanoengineering and Nanomanufacturing, 2013. **3**(1): p. 39-47.
41. Velhal, N.B., et al., Structural, dielectric and magnetic properties of nickel substituted cobalt ferrite nanoparticles: Effect of nickel concentration. AIP Advances, 2015. **5**(9): p. 097166.
42. Rani, R., et al., Electric and dielectric study of zinc substituted cobalt nanoferrites prepared by solution combustion method. American Journal of Nanomaterials, 2013. **1**(1): p. 9-12.
43. Bhise, R., S. Rathod, and A. Supekar, Dielectric, Magnetic, Electric and Structural Properties of Ni0. 2-Cox-Zn0. 8-x Ferrite Nanoparticles Synthesized by Sol-Gel Auto Combustion Method. International Journal of Advancements in Research & Technology, 2013. **2**: p. 1-6.

44. Kumar, K.V., et al., Structural properties and electrical conductivity of copper substituted nickel nano ferrites. International Journal of Applied Physics and Mathematics, 2014. **4**(2): p. 113.
45. Ali, A.A., et al., MWCNTs/carbon nano fibril composite papers for fuel cell and super capacitor applications. Journal of Electrostatics, 2015. **73**: p. 12-18.
46. Ahmad, R., et al., Improved electrical properties of cadmium substituted cobalt ferrites nano-particles for microwave application. Journal of magnetism and magnetic materials, 2016. **405**: p. 28-35.
47. Melo, R., et al., Magnetic ferrites synthesised using the microwave-hydrothermal method. Journal of Magnetism and Magnetic Materials, 2015. **381**: p. 109-115.
48. Klug, H.P. and L.E. Alexander, X-ray diffraction procedures. 1954.
49. Özdemir, Z.G., et al., Super-capacitive behavior of carbon nano tube doped 11-(4-cyanobiphenyl-4-oxy) undecan-1-ol. Journal of Molecular Liquids, 2015. **211**: p. 442-447.
50. "Scanning Electron Microscope A to Z." N.p., n.d.W.N.
51. Zhang, X., et al., One-step solvothermal synthesis of graphene/Mn3O4 nanocomposites and their electrochemical properties for supercapacitors. Materials Letters, 2012. **68**: p. 336-339.
52. Ying, Y. and P. Yu, Microprobing Structural Architecture Using Mid-Infrared Vibrational Molecular Spectroscopy, in Applications of Molecular Spectroscopy to Current Research in the Chemical and Biological Sciences. 2016, InTech.
53. Murugesan, C., M. Perumal, and G. Chandrasekaran, Structural, dielectric and magnetic properties of cobalt ferrite prepared using auto combustion and ceramic route. Physica B: Condensed Matter, 2014. **448**: p. 53-56.
54. Mirzaee, S., S.F. Shayesteh, and S. Mahdavifar, Anisotropy investigation of cobalt ferrite nanoparticles embedded in polyvinyl alcohol matrix: a Monte Carlo study. Polymer, 2014. **55**(16): p. 3713-3719.
55. Rosnan, R., et al., Effects of Mg substitution on the structural and magnetic properties of Co0. 5Ni0. 5− x Mg x Fe2O4 nanoparticle ferrites. Chinese Physics B, 2016. **25**(4): p. 047501.

56. Varma, M.C., et al., Estimating the Cation Distributions in Ferrites Using X-Ray, FT-IR, and Magnetization Measurements. Physics Research International, 2014. **2014**.
57. Naeem, M., et al., Structural, electrical and magnetic characterization of Ni–Mg spinel ferrites. Journal of Alloys and Compounds, 2009. **487**(1-2): p. 739-743.
58. Denton, A.R. and N.W. Ashcroft, Vegard's law. Physical review A, 1991. **43**(6): p. 3161.
59. Reshak, A., Dispersion of the second harmonic generation in GaNxAs1− x (x= 0.25, 0.5, 0.75) alloys. Journal of Alloys and Compounds, 2014. **589**: p. 213-217.
60. Rao, C.N.R., Chemical applications of infrared spectroscopy. 1963, Academic Press.
61. Levin, M. and M. Miller, Maxwell's" Treatise on Electricity and Magnetism". Soviet Physics Uspekhi, 1981. **24**(11): p. 904.
62. Kumar, A., P. Sharma, and D. Varshney, Structural, vibrational and dielectric study of Ni doped spinel Co ferrites: Co1− xNixFe2O4 (x= 0.0, 0.5, 1.0). Ceramics International, 2014. **40**(8): p. 12855-12860.
63. Yadav, G., et al., Enhancement in Magnetic and Dielectric Properties of Magnesium Ferrite by Lithium Substitution Applicable for High Frequency Shielding Material.
64. Chandra, K., S. Singhal, and S. Goyal, Magnetic and Mössbauer spectral studies of nano crystalline cobalt substituted magnesium ferrites (Mg x Co 1− x Fe 2 O 4), in ICAME 2007. 2008, Springer. p. 247-252.
65. Sharma, J., et al., Dielectric properties of nanocrystalline Co-Mg ferrites. Journal of Alloys and Compounds, 2015. **649**: p. 362-367.
66. Gabal, M., Y. Al Angari, and F. Al-Agel, Cr-substituted Ni–Zn ferrites via oxalate decomposition. Structural, electrical and magnetic properties. Journal of Magnetism and Magnetic Materials, 2015. **391**: p. 108-115.
67. John, H., et al., Conducting polyaniline composites as microwave absorbers. Polymer composites, 2007. **28**(5): p. 588-592.

68. Gul, I., et al., Optical, magnetic and electrical investigation of cobalt ferrite nanoparticles synthesized by co-precipitation route. Journal of alloys and compounds, 2010. **507**(1): p. 201-206.
69. Kumari, N., V. Kumar, and S. Singh, Structural, dielectric and magnetic investigations on Al 3+ substituted Zn-ferrospinels. RSC Advances, 2015. **5**(47): p. 37925-37934.
70. Cole, K.S. and R.H. Cole, Dispersion and absorption in dielectrics II. Direct current characteristics. The Journal of Chemical Physics, 1942. **10**(2): p. 98-105.
71. Kumari, R., et al., Rietveld refinement, impedance spectroscopy and magnetic properties of Bi0. 8Sr0. 2FeO3 substituted Na0. 5Bi0. 5TiO3 ceramics. Journal of Magnetism and Magnetic Materials, 2016. **414**: p. 1-9.
72. Ye, H., R.B. Jackman, and P. Hing, Spectroscopic impedance study of nanocrystalline diamond films. Journal of applied physics, 2003. **94**(12): p. 7878-7882.
73. Kaiser, M., Electrical conductivity and complex electric modulus of titanium doped nickel–zinc ferrites. Physica B: Condensed Matter, 2012. **407**(4): p. 606-613.